Journal of Computational Physics 417 (2020) 109583

Contents lists available at ScienceDirect

Journal of Computational Physics

www.elsevier.com/locate/jcp

A Hermite WENO scheme with artificial linear weights for hyperbolic conservation laws ☆

Zhuang Zhao [a], Jianxian Qiu [b,*]

[a] School of Mathematical Sciences, Xiamen University, Xiamen, Fujian 361005, PR China
[b] School of Mathematical Sciences and Fujian Provincial Key Laboratory of Mathematical Modeling and High-Performance Scientific Computing, Xiamen University, Xiamen, Fujian 361005, PR China

ARTICLE INFO

Article history:
Received 30 January 2020
Received in revised form 17 May 2020
Accepted 18 May 2020
Available online 25 May 2020

Keywords:
Hermite WENO scheme
Hyperbolic conservation laws
Unequal size spatial stencil
Hybrid
Discontinuous Galerkin method

ABSTRACT

In this paper, a fifth-order Hermite weighted essentially non-oscillatory (HWENO) scheme with artificial linear weights is proposed for one and two dimensional hyperbolic conservation laws, where the zeroth-order and the first-order moments are used in the spatial reconstruction. We construct the HWENO methodology using a nonlinear convex combination of a high degree polynomial with several low degree polynomials, and the associated linear weights can be any artificial positive numbers with only requirement that their summation equals one. The one advantage of the HWENO scheme is its simplicity and easy extension to multi-dimension in engineering applications for we can use any artificial linear weights which are independent on geometry of mesh. The another advantage is its higher order numerical accuracy using less candidate stencils for two dimensional problems. In addition, the HWENO scheme still keeps the compactness as only immediate neighbor information is needed in the reconstruction and has high efficiency for directly using linear approximation in the smooth regions. In order to avoid nonphysical oscillations nearby strong shocks or contact discontinuities, we adopt the thought of limiter for discontinuous Galerkin method to control the spurious oscillations. Some benchmark numerical tests are performed to demonstrate the capability of the proposed scheme.

1. Introduction

In this paper, we develop a fifth order Hermite weighted essentially non-oscillatory (HWENO) scheme with artificial linear weights for one and two dimensional nonlinear hyperbolic conservation laws. The idea of HWENO scheme is similar to that of weighted essentially non-oscillatory (WENO) scheme which have been widely applied for computational dynamics fluids. In 1994, the first WENO scheme was proposed by Liu, Osher and Chan [25] mainly in terms of ENO scheme [19,17,18], in which they combined all candidate stencils by a nonlinear convex manner to obtain higher order accuracy in smooth regions, then, in 1996, Jiang and Shu [22] constructed the third and fifth-order finite difference WENO schemes in multi-space dimension, where they gave a general definition for smoothness indicators and nonlinear weights. Since then, WENO schemes have been further developed in [21,26,37,6,46]. However, if we design a higher order accuracy WENO scheme, we

☆ The research is partly supported by Science Challenge Project, No. TZ2016002 and NSAF grant U1630247.
* Corresponding author.
E-mail addresses: zzhao@stu.xmu.edu.cn (Z. Zhao), jxqiu@xmu.edu.cn (J. Qiu).

https://doi.org/10.1016/j.jcp.2020.109583
0021-9991/

need to enlarge the stencil. In order to keep the compactness of the scheme, Qiu and Shu [31,32] gave a new option by evolving both with the solution and its derivative, which were termed as Hermite WENO (HWENO) schemes.

HWENO schemes would have higher order accuracy than WENO schemes with the same reconstructed stencils. As the solutions of nonlinear hyperbolic conservation laws often contain discontinuities, its derivatives or first order moments would be relatively large nearby discontinuities. Hence, the HWENO schemes presented in [31,32,45,39,29,43,40,11] used different stencils to discretize the space for the original and derivative equations, respectively. In one sense, these HWENO schemes can be seen as an extension by DG methods, and Dumbser et al. [13] gave a general and unified framework to define the numerical scheme extended by DG method, termed as $P_N P_M$ method. But the derivatives or the first order moments were still used straightforwardly nearby the discontinuities, which would be less robust for problems with strong shocks. Such as the first HWENO schemes [31,32] failed to simulate the double Mach and the step forward problems, then, Zhu and Qiu [45] solved this problem by using a new procedure to reconstruct the derivative terms, while Cai et al. [11] employed additional positivity-preserving manner. Overall, only using different stencils to discretize the space is not enough to overcome the effect of the derivatives or the first order moments near the discontinuities. Hence, we took the thought of limiter for discontinuous Galerkin (DG) method [10] to modify the first order moments nearby the discontinuities of the solution in [44], meanwhile, we also noticed that many hybrid WENO schemes [30,20,7,8,28,51] employed linear schemes directly in the smooth regions, while still used WENO schemes in the discontinuous regions, which can increase the efficiency obviously, therefore, in [44], we directly used high order linear approximation in the smooth regions, while modified the first order moments on the troubled-cells and employed HWENO reconstruction on the interface. The methodology for the modification is similar to the priori finite volume WENO [33,2,50] and HWENO [31,32,24,52] limiters, while the posteriori limiter technique can refer to the Multidimensional Optimal Order Detection (MOOD) methods [9,14,15,3]. The hybrid HWENO scheme [44] had high efficiency and resolution with non-physical oscillations, but it still had a drawback of that the linear weights were dependent on geometry of the mesh and point where the reconstruction was performed, and they were not easy to be computed, especially for multi-dimensional problems with unstructured meshes. For example, in [44] we needed to compute the linear weights at twelve points in one cell by a least square methodology with eight small stencils for two dimensional problems, in which the numerical accuracy was only the fourth order. Moreover, if we solve the problems for unstructured meshes, the linear weights would be more difficult to calculate, and the negative weights may appear or there is non-existence of the linear weights for some cases. In order to overcome the drawback, Zhu and Qiu [46] presented a new simple WENO scheme in the finite difference framework, which had a convex combination of a fourth degree polynomial and other two linear polynomials by using any artificial positive linear weights (the sum equals one). Then the method was extended to finite volume methods both in structured and unstructured meshes [5,47,12,48,49,4].

In this paper, following the idea of the new type WENO [46,5,47,12,48,49,4], hybrid WENO [30,20,7,8,28,51] and hybrid HWENO [44] schemes, we develop the new hybrid HWENO scheme in which we use a nonlinear convex combination of a high degree polynomial with several low degree polynomials and the linear weights can be any artificial positive numbers with the only constraint that their sum is one. The procedures of the new hybrid HWENO scheme are: firstly, we modify the first order moments using the new HWENO limiter methodology in the troubled-cells, which are identified by the KXRCF troubled-cell indicator [23]. Then, for the space discretization, if the cell is identified as a troubled-cell, we would use the new HWENO reconstruction at the points on the interface; otherwise we employ linear approximation at the interface points straightforwardly. And we directly use high order linear approximation at the internal points for all cells. Finally, the third order TVD Runge-Kutta method [38] is applied for the time discretization. Particularly, only the new HWENO reconstructions need to be performed on local characteristic directions for systems. In addition, the new hybrid HWENO scheme inherits the advantages of [44], such as non-physical oscillations for using the idea of limiter for discontinuous Galerkin (DG) method, high efficiency for employing linear approximation straightforwardly in the smooth regions, and compactness as only immediate neighbor information is needed, meanwhile, it gets smaller numerical errors on the same meshes and has higher order numerical accuracy for two dimensional problems.

The organization of the paper is as follows: in Section 2, we introduce the detailed implementation of the new hybrid HWENO scheme in the one and two dimensional cases. In Section 3, some benchmark numerical are performed to illustrate the numerical accuracy, efficiency, resolution and robustness of proposed scheme. Concluding remarks are given in Section 4.

2. Description of Hermite WENO scheme with artificial linear weights

In this section, we present the construction procedures of the hybrid HWENO scheme with artificial linear weights for one and two dimensional hyperbolic conservation laws, which is the fifth order accuracy both in the one and two dimensional cases.

2.1. One dimensional case

At first, we consider one dimensional scalar hyperbolic conservation laws

$$\begin{cases} u_t + f(u)_x = 0, \\ u(x,0) = u_0(x). \end{cases} \tag{2.1}$$

The computing domain is divided by uniform meshes $I_i = [x_{i-1/2}, x_{i+1/2}]$ for simplicity, and the mesh center x_i is $\frac{x_{i-1/2}+x_{i+1/2}}{2}$ with the mesh size $\Delta x = x_{i+1/2} - x_{i-1/2}$.

As the variables of our designed HWENO scheme are the zeroth and first order moments, we multiply the governing equation (2.1) by $\frac{1}{\Delta x}$ and $\frac{x-x_i}{(\Delta x)^2}$, respectively, then, integrate them over I_i, and apply the integration by parts, having

$$\begin{cases} \dfrac{1}{\Delta x}\displaystyle\int_{I_i} u_t dx = -\frac{1}{\Delta x}\left[f\left(u(x_{i+1/2},t)\right) - f\left(u(x_{i+1/2},t)\right)\right], \\ \dfrac{1}{\Delta x}\displaystyle\int_{I_i} u_t \frac{x-x_i}{\Delta x} dx = -\frac{1}{2\Delta x}\left[f\left(u(x_{i-1/2},t)\right) + f\left(u(x_{i+1/2},t)\right)\right] + \frac{1}{(\Delta x)^2}\int_{I_i} f(u)dx. \end{cases}$$

Later, we exchange the space and the time derivatives, and employ the numerical flux to approximate the value of the flux at the interface, then, the semi-discrete finite volume HWENO scheme is

$$\begin{cases} \dfrac{d\overline{u}_i(t)}{dt} = -\dfrac{1}{\Delta x}\left(\hat{f}_{i+1/2} - \hat{f}_{i-1/2}\right), \\ \dfrac{d\overline{v}_i(t)}{dt} = -\dfrac{1}{2\Delta x}\left(\hat{f}_{i-1/2} + \hat{f}_{i+1/2}\right) + \dfrac{1}{\Delta x}F_i(u), \end{cases} \tag{2.2}$$

where $\overline{u}_i(t)$ is the zeroth order moment in I_i as $\frac{1}{\Delta x}\int_{I_i} u(x,t)dx$ and $\overline{v}_i(t)$ is the first order moment in I_i as $\frac{1}{\Delta x}\int_{I_i} u(x,t)\frac{x-x_i}{\Delta x}dx$. The initial conditions are $\overline{u}_i(0) = \frac{1}{\Delta x}\int_{I_i} u_0(x)dx$ and $\overline{v}_i(0) = \frac{1}{\Delta x}\int_{I_i} u_0(x)\frac{x-x_i}{\Delta x}dx$. $F_i(u)$ is the integra average value for the flux $f(u)$ over I_i as $\frac{1}{\Delta x}\int_{I_i} f(u)dx$. $\hat{f}_{i+1/2}$ is the numerical flux to approximate the value of the flux $f(u)$ at the interface point $x_{i+1/2}$, which is defined by the Lax-Friedrichs numerical flux method, and the explicit expression is

$$\hat{f}_{i+1/2} = \frac{1}{2}\left(f(u^-_{i+1/2}) + f(u^+_{i+1/2})\right) - \frac{\alpha}{2}\left(u^+_{i+1/2} - u^-_{i+1/2}\right),$$

in which $\alpha = \max_u |f'(u)|$. $F_i(u)$ is approximated by a four-point Gauss-Lobatto quadrature formula:

$$F_i(u) = \frac{1}{\Delta x}\int_{I_i} f(u)dx \approx \sum_{l=1}^{4} \omega_l f(u(x_l^G, t)),$$

where the weights are $\omega_1 = \omega_4 = \frac{1}{12}$ and $\omega_2 = \omega_3 = \frac{5}{12}$, and the quadrature points on the cell I_i are

$$x_1^G = x_{i-1/2}, \quad x_2^G = x_{i-\sqrt{5}/10}, \quad x_3^G = x_{i+\sqrt{5}/10}, \quad x_4^G = x_{i+1/2},$$

in which x_{i+a} is $x_i + a\Delta x$.

Now, we first present the detailed procedures of the spatial reconstruction for HWENO scheme in Steps 1 and 2, then, we introduce the method of time discretization in Step 3.

Step 1. Identify the troubled-cell and modify the first order moment in the troubled-cell.

Troubled-cell means that the solution of the equation in the cell may be discontinuous, and in [34], Qiu and Shu investigated different troubled-cell indicators for Runge-Kutta discontinuous Galerkin methods, then, we choose the KXRCF troubled-cell indicator [23] to identify the troubled-cell suggested by [34]. The construction of the KXRCF troubled-cell indicator [23] was based on the strong super-convergence phenomena for the smooth DG solutions at outflow boundaries, which is desirable for hyperbolic conservation laws as it can balance the ability of capturing discontinuities and the efficiency of the DG scheme well shown in [34], and its parameter C_k is insensitive usually taken as 1. Meanwhile, it would mark a lot more troubled cells than necessary for high-order DG methods, but it seems to mark the troubled cells appropriately for our scheme shown in the numerical results as the degree of the polynomial u_h used in the troubled-cell indicator is 2. Actually, the KXRCF troubled-cell indicator [23] is only a choice, other troubled-cell indicators are possible. Such as the relaxed Discrete Maximum Principle (RDMP) as the troubled-cell indicator for Multi-dimensional Optimal Order Detection (MOOD) method [3], the multi-wavelet troubled-cell indicator [41], the troubled-cell indication without PDE sensitive parameters [16], the artificial neural network troubled-cell indicator [35], and the flattener troubled-cell indicator [1] for Arbitrary-Lagrangian-Eulerian (ALE) $P_N P_M$ scheme [2]. In addition, the explicit procedures for the KXRCF troubled-cell indicator were given in the hybrid HWENO scheme [44], then, if the cell I_i is identified as a troubled cell, we would also mark its neighbors as troubled cells as [44], then, we modify the first order moment $\overline{v}_i$ in the troubled cells by the following procedures.

We use the thought of HWENO limiter [31] to modify the first order moment, but the modification for the first order moment is based on a convex combination of a fourth degree polynomial with two linear polynomials. Firstly, we give a large stencil $S_0 = \{I_{i-1}, I_i, I_{i+1}\}$ and two small stencils $S_1 = \{I_{i-1}, I_i\}$, $S_2 = \{I_i, I_{i+1}\}$, then, we obtain a quartic polynomial $p_0(x)$ on S_0, as

$$\frac{1}{\Delta x}\int_{I_{i+j}} p_0(x)dx=\overline{u}_{i+j},\ j=-1,0,1,\quad \frac{1}{\Delta x}\int_{I_{i+j}} p_0(x)\frac{x-x_{i+j}}{\Delta x}dx=\overline{v}_{i+j},\ j=-1,1,$$

and get two linear polynomials $p_1(x), p_2(x)$ on S_1, S_2, respectively, satisfying

$$\frac{1}{\Delta x}\int_{I_{i+j}} p_1(x)dx=\overline{u}_{i+j},\quad j=-1,0,$$
$$\frac{1}{\Delta x}\int_{I_{i+j}} p_2(x)dx=\overline{u}_{i+j},\quad j=0,1.$$

We use these three polynomials to reconstruct $\overline{v}_i=\frac{1}{\Delta x}\int_{I_i} u(x)\frac{x-x_i}{\Delta x}dx$, and their explicit results are

$$\frac{1}{\Delta x}\int_{I_i} p_0(x)\frac{x-x_i}{\Delta x}dx=\frac{5}{76}\overline{u}_{i+1}-\frac{5}{76}\overline{u}_{i-1}-\frac{11}{38}\overline{v}_{i-1}-\frac{11}{38}\overline{v}_{i+1},$$
$$\frac{1}{\Delta x}\int_{I_i} p_1(x)\frac{x-x_i}{\Delta x}dx=\frac{1}{12}\overline{u}_i-\frac{1}{12}\overline{u}_{i-1},$$
$$\frac{1}{\Delta x}\int_{I_i} p_2(x)\frac{x-x_i}{\Delta x}dx=\frac{1}{12}\overline{u}_{i+1}-\frac{1}{12}\overline{u}_i.$$

For simplicity, we define q_n as $\frac{1}{\Delta x}\int_{I_i} p_n(x)\frac{x-x_i}{\Delta x}dx$ in the next procedures. With the similar idea of the central WENO schemes [26,27] and the new WENO schemes [46–49], we rewrite q_0 as:

$$q_0=\gamma_0\left(\frac{1}{\gamma_0}q_0-\frac{\gamma_1}{\gamma_0}q_1-\frac{\gamma_2}{\gamma_0}q_2\right)+\gamma_1 q_1+\gamma_2 q_2. \tag{2.3}$$

We can notice that equation (2.3) is always satisfied for any choice of γ_0, γ_1, γ_2 with $\gamma_0\neq 0$. To make the next WENO procedure be stable, the linear weights would be positive with $\gamma_0+\gamma_1+\gamma_2=1$, then, we calculate the smoothness indicators β_n to measure how smooth the functions $p_n(x)$ in the cell I_i, and we use the same definition as in [22],

$$\beta_n=\sum_{\alpha=1}^{r}\int_{I_i}\Delta x^{2\alpha-1}\left(\frac{d^\alpha p_n(x)}{dx^\alpha}\right)^2dx,\quad n=0,1,2, \tag{2.4}$$

where r is the degree of the polynomials $p_n(x)$, then, the expressions for the smoothness indicators are

$$\begin{cases}
\beta_0=\left(\frac{29}{38}\overline{u}_{i-1}-\frac{29}{38}\overline{u}_{i+1}+\frac{60}{19}\overline{v}_{i-1}+\frac{60}{19}\overline{v}_{i+1}\right)^2+\left(\frac{9}{4}\overline{u}_{i-1}-\frac{9}{2}\overline{u}_i+\frac{9}{4}\overline{u}_{i+1}+\frac{15}{2}\overline{v}_{i-1}-\frac{15}{2}\overline{v}_{i+1}\right)^2+\\
\qquad\frac{3905}{1444}\left(\overline{u}_{i-1}-\overline{u}_{i+1}+12\overline{v}_{i-1}+12\overline{v}_{i+1}\right)^2+\frac{1}{12}\left(\frac{5}{2}\overline{u}_{i-1}-5\overline{u}_i+\frac{5}{2}\overline{u}_{i+1}+9\overline{v}_{i-1}-9\overline{v}_{i+1}\right)^2+\\
\qquad\frac{109341}{448}\left(\overline{u}_{i-1}-2\overline{u}_i+\overline{u}_{i+1}+6\overline{v}_{i-1}-6\overline{v}_{i+1}\right)^2,\\
\beta_1=\left(\overline{u}_i-\overline{u}_{i-1}\right)^2,\\
\beta_2=\left(\overline{u}_{i+1}-\overline{u}_i\right)^2.
\end{cases}$$

Later, we use a new parameter τ to measure the absolute difference between β_0, β_1 and β_2, which is also can be seen in these new WENO schemes [46–49],

$$\tau=\left(\frac{|\beta_0-\beta_1|+|\beta_0-\beta_2|}{2}\right)^2, \tag{2.5}$$

and the nonlinear weights are defined as

$$\omega_n=\frac{\bar{\omega}_n}{\sum_{\ell=0}^{2}\bar{\omega}_\ell},\ \text{with}\ \bar{\omega}_n=\gamma_n\left(1+\frac{\tau}{\beta_n+\varepsilon}\right),\ n=0,1,2,$$

where $\varepsilon=10^{-6}$ is to avoid the denominator by zero. Finally, the first order moment $\overline{v}_i$ is modified by

$$\overline{v}_i=\omega_0\left(\frac{1}{\gamma_0}q_0-\sum_{n=1}^{2}\frac{\gamma_n}{\gamma_0}q_n\right)+\sum_{n=1}^{2}\omega_n q_n.$$

Notice that we just replace the linear weights in equation (2.3) by the nonlinear weights, and the accuracy of the modification depends on the accuracy of the high degree reconstructed polynomial. The modification for the first order moment $\overline{v}_i$ would be the fifth order accuracy in the smooth regions, and more detailed derivation can refer to the literature [47].

Step 2. Reconstruct the values of the solutions u at the four Gauss-Lobatto points.

We use the same stencils S_0, S_1, S_2 as Step 1, then, if the cell I_i is identified as a troubled cell, we would reconstruct $u^{\pm}_{i\mp1/2}$ using the HWENO methodology in Step 2.1; otherwise we directly reconstruct $u^{\pm}_{i\mp1/2}$ by the linear approximation method described in Step 2.2. And the reconstruction procedure for $u_{i\pm\sqrt{5}/10}$ is given in Step 2.3.

Step 2.1. The new HWENO reconstruction for $u^{\pm}_{i\mp1/2}$.

If the cell I_i is identified as a troubled cell, $u^{\pm}_{i\mp1/2}$ is reconstructed by the next HWENO procedure. For simplicity, we only present the detailed procedure of the reconstruction for $u^{-}_{i+1/2}$, while the reconstruction for $u^{+}_{i-1/2}$ is mirror symmetric with respect to x_i. Notice that we have modified the first order moment in the troubled-cells, then, we would use these information here. We now reconstruct three polynomials $p_0(x), p_1(x), p_2(x)$ on S_0, S_1, S_2, respectively, satisfying

$$\begin{aligned}
&\frac{1}{\Delta x}\int_{I_{i+j}} p_0(x)dx=\overline{u}_{i+j},\ \frac{1}{\Delta x}\int_{I_{i+j}} p_0(x)\frac{x-x_{i+j}}{\Delta x}dx=\overline{v}_{i+j},\quad j=-1,0,1,\\
&\frac{1}{\Delta x}\int_{I_{i+j}} p_1(x)dx=\overline{u}_{i+j},\ j=-1,0,\quad \frac{1}{\Delta x}\int_{I_i} p_1(x)\frac{x-x_i}{\Delta x}dx=\overline{v}_i,\\
&\frac{1}{\Delta x}\int_{I_{i+j}} p_2(x)dx=\overline{u}_{i+j},\ j=0,1,\quad \frac{1}{\Delta x}\int_{I_i} p_2(x)\frac{x-x_i}{\Delta x}dx=\overline{v}_i.
\end{aligned}$$

In terms of the above requirements, we first give the values of these polynomials at the point $x_{i+1/2}$, following as

$$\begin{aligned}
p_0(x_{i+1/2})&=\frac{13}{108}\overline{u}_{i-1}+\frac{7}{12}\overline{u}_i+\frac{8}{27}\overline{u}_{i+1}+\frac{25}{54}\overline{v}_{i-1}+\frac{241}{54}\overline{v}_i-\frac{28}{27}\overline{v}_{i+1},\\
p_1(x_{i+1/2})&=\frac{1}{6}\overline{u}_{i-1}+\frac{5}{6}\overline{u}_i+8\overline{v}_i,\\
p_2(x_{i+1/2})&=\frac{5}{6}\overline{u}_i+\frac{1}{6}\overline{u}_{i+1}+4\overline{v}_i.
\end{aligned}$$

Using the next new HWENO methodology, we can use any positive linear weights satisfying $\gamma_0+\gamma_1+\gamma_2=1$, then, we compute the smoothness indicators β_n in the same ways, and the formula of the smoothness indicators has been given in (2.4) of Step 1, then, their expressions are given as follows,

$$\begin{cases}
\beta_0 =(\frac{19}{108}\overline{u}_{i-1}-\frac{19}{108}\overline{u}_{i+1}+\frac{31}{54}\overline{v}_{i-1}-\frac{241}{27}\overline{v}_i+\frac{31}{54}\overline{v}_{i+1})^2+(\frac{9}{4}\overline{u}_{i-1}-\frac{9}{2}\overline{u}_i+\frac{9}{4}\overline{u}_{i+1}+\\
\quad\frac{15}{2}\overline{v}_{i-1}-\frac{15}{2}\overline{v}_{i+1})^2+(\frac{70}{9}\overline{u}_{i-1}-\frac{70}{9}\overline{u}_{i+1}+\frac{200}{9}\overline{v}_{i-1}+\frac{1280}{9}\overline{v}_i+\frac{200}{9}\overline{v}_{i+1})^2+\\
\quad\frac{1}{12}(\frac{5}{2}\overline{u}_{i-1}-5\overline{u}_i+\frac{5}{2}\overline{u}_{i+1}+9\overline{v}_{i-1}-9\overline{v}_{i+1})^2+\frac{1}{12}(\frac{175}{18}\overline{u}_{i-1}-\frac{175}{18}\overline{u}_{i+1}+\frac{277}{9}\overline{v}_{i-1}+\\
\quad\frac{1546}{9}\overline{v}_i+\frac{277}{9}\overline{v}_{i+1})^2+\frac{1}{180}(\frac{95}{18}\overline{u}_{i-1}-\frac{95}{18}\overline{u}_{i+1}+\frac{155}{9}\overline{v}_{i-1}+\frac{830}{9}\overline{v}_i+\frac{155}{9}\overline{v}_{i+1})^2+\\
\quad\frac{109341}{175}(\frac{5}{8}\overline{u}_{i-1}-\frac{5}{4}\overline{u}_i+\frac{5}{8}\overline{u}_{i+1}+\frac{15}{4}\overline{v}_{i-1}-\frac{15}{4}\overline{v}_{i+1})^2+\frac{27553933}{1764}(\frac{35}{36}\overline{u}_{i-1}-\frac{35}{36}\overline{u}_{i+1}+\\
\quad\frac{77}{18}\overline{v}_{i-1}+\frac{133}{9}\overline{v}_i+\frac{77}{18}\overline{v}_{i+1})^2,\\
\beta_1 =144\overline{v}_i^2+\frac{13}{3}(\overline{u}_{i-1}-\overline{u}_i+12\overline{v}_i)^2,\\
\beta_2 =144\overline{v}_i^2+\frac{13}{3}(\overline{u}_i-\overline{u}_{i+1}+12\overline{v}_i)^2.
\end{cases}$$

We bring the same parameter τ to define the absolute difference between β_0, β_1 and β_2, and the formula is given in (2.5), then, the nonlinear weights are computed as

$$\omega_n=\frac{\bar{\omega}_n}{\sum_{\ell=0}^{2}\bar{\omega}_\ell},\ \text{with}\ \bar{\omega}_n=\gamma_n(1+\frac{\tau}{\beta_n+\varepsilon}),\ n=0,1,2.$$

Here, ε is a small positive number taken as 10^{-6}. Finally, the value of $u^{-}_{i+1/2}$ is reconstructed by

$$u^{-}_{i+1/2} = \omega_0 \left(\frac{1}{\gamma_0} p_0(x_{i+1/2}) - \sum_{n=1}^{2} \frac{\gamma_n}{\gamma_0} p_n(x_{i+1/2}) \right) + \sum_{n=1}^{2} \omega_n p_n(x_{i+1/2}).$$

Step 2.2. The linear approximation for $u^{\mp}_{i\pm1/2}$.

If the cell I_i is not a troubled cell, we will use the linear approximation for $u^{\mp}_{i\pm1/2}$, which means we only need to use the high degree polynomial $p_0(x)$ obtained in Step 2.1, then, we have

$$u^{+}_{i-1/2} = p_0(x_{i-1/2}) = \frac{8}{27}\overline{u}_{i-1} + \frac{7}{12}\overline{u}_i + \frac{13}{108}\overline{u}_{i+1} + \frac{28}{27}\overline{v}_{i-1} - \frac{241}{54}\overline{v}_i - \frac{25}{54}\overline{v}_{i+1},$$

and

$$u^{-}_{i+1/2} = p_0(x_{i+1/2}) = \frac{13}{108}\overline{u}_{i-1} + \frac{7}{12}\overline{u}_i + \frac{8}{27}\overline{u}_{i+1} + \frac{25}{54}\overline{v}_{i-1} + \frac{241}{54}\overline{v}_i - \frac{28}{27}\overline{v}_{i+1}.$$

Step 2.3. The linear approximation for $u_{i\pm\sqrt{5}/10}$.

We would reconstruct $u_{i\pm\sqrt{5}/10}$ using the linear approximation for all cells, then, $u_{i\pm\sqrt{5}/10}$ are approximated by

$$\begin{aligned} u_{i-\sqrt{5}/10} = p_0(x_{i-\sqrt{5}/10}) = &-(\frac{101}{5400}\sqrt{5} + \frac{1}{24})\overline{u}_{i-1} + \frac{13}{12}\overline{u}_i + (\frac{101}{5400}\sqrt{5} - \frac{1}{24})\overline{u}_{i+1} - \\ &(\frac{3}{20} + \frac{841}{13500}\sqrt{5})\overline{v}_{i-1} - \frac{10289}{6750}\sqrt{5}\overline{v}_i + (\frac{3}{20} - \frac{841}{13500}\sqrt{5})\overline{v}_{i+1}, \end{aligned}$$

and

$$\begin{aligned} u_{i+\sqrt{5}/10} = p_0(x_{i+\sqrt{5}/10}) = &(\frac{101}{5400}\sqrt{5} - \frac{1}{24})\overline{u}_{i-1} + \frac{13}{12}\overline{u}_i - (\frac{101}{5400}\sqrt{5} + \frac{1}{24})\overline{u}_{i+1} + \\ &(\frac{841}{13500}\sqrt{5} - \frac{3}{20})\overline{v}_{i-1} + \frac{10289}{6750}\sqrt{5}\overline{v}_i + (\frac{3}{20} + \frac{841}{13500}\sqrt{5})\overline{v}_{i+1}. \end{aligned}$$

Step 3. Discretize the semi-discrete scheme (2.2) in time by the third order TVD Runge-Kutta method [38]

$$\begin{cases} u^{(1)} &= u^n + \Delta t L(u^n), \\ u^{(2)} &= \frac{3}{4}u^n + \frac{1}{4}u^{(1)} + \frac{1}{4}\Delta t L(u^{(1)}), \\ u^{(n+1)} &= \frac{1}{3}u^n + \frac{2}{3}u^{(2)} + \frac{2}{3}\Delta t L(u^{(2)}). \end{cases} \tag{2.6}$$

Remark 1. The KXRCF troubled-cell indicator can catch the discontinuities well. For one dimensional scalar equation, the solution u is defined as the indicator variable, then $\overrightarrow{v}$ is $f'(u)$. For one dimensional Euler equations, the density ρ and the energy E are set as the indicator variables, respectively, then $\overrightarrow{v}$ is the velocity μ of the fluid.

Remark 2. For the systems, such as the one dimensional compressible Euler equations, all HWENO procedures are performed on the local characteristic directions to avoid the oscillations nearby discontinuities, while the linear approximation procedures are computed in each component straightforwardly.

2.2. Two dimensional case

We first consider two dimensional scalar hyperbolic conservation laws

$$\begin{cases} u_t + f(u)_x + g(u)_y = 0, \\ u(x, y, 0) = u_0(x, y), \end{cases} \tag{2.7}$$

then, we divide the computing domain by uniform meshes $I_{i,j} = [x_{i-1/2}, x_{i+1/2}] \times [y_{j-1/2}, y_{j+1/2}]$ for simplicity. The mesh sizes are $\Delta x = x_{i+1/2} - x_{i-1/2}$ in the x direction and $\Delta y = y_{j+1/2} - y_{j-1/2}$ in the y direction. The cell center (x_i, y_j) is $(\frac{x_{i-1/2}+x_{i+1/2}}{2}, \frac{y_{j-1/2}+y_{j+1/2}}{2})$. $x_i + a\Delta x$ is simplified as x_{i+a} and $y_j + b\Delta y$ is set as y_{j+b}.

Since the variables of the HWENO scheme are the zeroth and first order moments, we multiply the governing equation (2.7) by $\frac{1}{\Delta x \Delta y}$, $\frac{x-x_i}{(\Delta x)^2 \Delta y}$ and $\frac{y-y_j}{\Delta x (\Delta y)^2}$ on both sides, respectively, then, we integrate them over $I_{i,j}$ and apply the integration by parts, having

$$
\begin{cases}
\dfrac{1}{\Delta x\Delta y}\displaystyle\int_{I_{i,j}} u_t dxdy = -\dfrac{1}{\Delta x\Delta y}\int_{y_{j-1/2}}^{y_{j+1/2}} \left[f\left(u(x_{i+1/2},y,t)\right) - f\left(u(x_{i-1/2},y,t)\right)\right]dy \\
\quad -\dfrac{1}{\Delta x\Delta y}\displaystyle\int_{x_{i-1/2}}^{x_{i+1/2}} \left[g\left(u(x,y_{j+1/2},t)\right) - g\left(u(x,y_{j-1/2},t)\right)\right]dx, \\
\dfrac{1}{\Delta x\Delta y}\displaystyle\int_{I_{i,j}} u_t\dfrac{x-x_i}{\Delta x}dxdy = -\dfrac{1}{2\Delta x\Delta y}\int_{y_{j-1/2}}^{y_{j+1/2}} \left[f\left(u(x_{i-1/2},y,t)\right) + f\left(u(x_{i+1/2},y,t)\right)\right]dy \\
\quad +\dfrac{1}{(\Delta x)^2\Delta y}\displaystyle\int_{I_{i,j}} f(u)dxdy - \dfrac{1}{\Delta x\Delta y}\int_{x_{i-1/2}}^{x_{i+1/2}} \left[g\left(u(x,y_{j+1/2},t)\right) - g\left(u(x,y_{j-1/2},t)\right)\right]\dfrac{(x-x_i)}{\Delta x}dx, \\
\dfrac{1}{\Delta x\Delta y}\displaystyle\int_{I_{i,j}} u_t\dfrac{y-y_j}{\Delta y}dxdy = -\dfrac{1}{\Delta x\Delta y}\int_{y_{j-1/2}}^{y_{j+1/2}} \left[f\left(u(x_{i+1/2},y,t)\right) - f\left(u(x_{i-1/2},y,t)\right)\right]\dfrac{(y-y_j)}{\Delta y}dy \\
\quad -\dfrac{1}{2\Delta x\Delta y}\displaystyle\int_{x_{i-1/2}}^{x_{i+1/2}} \left[g\left(u(x,y_{j-1/2},t)\right) + g\left(u(x,y_{j+1/2},t)\right)\right]dx + \dfrac{1}{\Delta x(\Delta y)^2}\int_{I_{i,j}} g(u)dxdy.
\end{cases}
$$

Next, we exchange the space and the time derivatives, and approximate the values of the fluxes at the points on the interface of $I_{i,j}$ by the numerical fluxes, then, the semi-discrete finite volume HWENO scheme is

$$
\begin{cases}
\dfrac{d\overline{u}_{i,j}(t)}{dt} = -\dfrac{1}{\Delta x\Delta y}\displaystyle\int_{y_{j-1/2}}^{y_{j+1/2}} \left[\hat{f}\left(u(x_{i+1/2},y)\right) - \hat{f}\left(u(x_{i-1/2},y)\right)\right]dy \\
\qquad\qquad -\dfrac{1}{\Delta x\Delta y}\displaystyle\int_{x_{i-1/2}}^{x_{i+1/2}} \left[\hat{g}\left(u(x,y_{j+1/2})\right) - \hat{g}\left(u(x,y_{j-1/2})\right)\right]dx, \\
\dfrac{d\overline{v}_{i,j}(t)}{dt} = -\dfrac{1}{2\Delta x\Delta y}\displaystyle\int_{y_{j-1/2}}^{y_{j+1/2}} \left[\hat{f}\left(u(x_{i-1/2},y)\right) + \hat{f}\left(u(x_{i+1/2},y)\right)\right]dy + \dfrac{1}{\Delta x}F_{i,j}(u) \\
\qquad\qquad -\dfrac{1}{\Delta x\Delta y}\displaystyle\int_{x_{i-1/2}}^{x_{i+1/2}} \left[\hat{g}\left(u(x,y_{j+1/2})\right) - \hat{g}\left(u(x,y_{j-1/2})\right)\right]\dfrac{(x-x_i)}{\Delta x}dx, \\
\dfrac{d\overline{w}_{i,j}(t)}{dt} = -\dfrac{1}{\Delta x\Delta y}\displaystyle\int_{y_{j-1/2}}^{y_{j+1/2}} \left[\hat{f}\left(u(x_{i+1/2},y)\right) - \hat{f}\left(u(x_{i-1/2},y)\right)\right]\dfrac{(y-y_j)}{\Delta y}dy \\
\qquad\qquad -\dfrac{1}{2\Delta x\Delta y}\displaystyle\int_{x_{i-1/2}}^{x_{i+1/2}} \left[\hat{g}\left(u(x,y_{j-1/2})\right) + \hat{g}\left(u(x,y_{j+1/2})\right)\right]dx + \dfrac{1}{\Delta y}G_{i,j}(u).
\end{cases}
\tag{2.8}
$$

Here, $\overline{u}_{i,j}(t)$ is the zeroth order moment defined as $\frac{1}{\Delta x\Delta y}\int_{I_{i,j}} u(x,y,t)dxdy$; $\overline{v}_{i,j}(t)$ and $\overline{w}_{i,j}(t)$ are the first order moments in the x and y directions taken as $\frac{1}{\Delta x\Delta y}\int_{I_{i,j}} u(x,y,t)\frac{x-x_i}{\Delta x}dxdy$ and $\frac{1}{\Delta x\Delta y}\int_{I_{i,j}} u(x,y,t)\frac{y-y_j}{\Delta y}dxdy$, respectively. The initial conditions are $\overline{u}_{i,j}(0) = \frac{1}{\Delta x\Delta y}\int_{I_{i,j}} u_0(x,y)dxdy$, $\overline{v}_{i,j}(0) = \frac{1}{\Delta x\Delta y}\int_{I_{i,j}} u_0(x,y)\frac{x-x_i}{\Delta x}dxdy$ and $\overline{w}_{i,j}(0) = \frac{1}{\Delta x\Delta y}\int_{I_{i,j}} u_0(x,y)\frac{y-y_j}{\Delta y}dxdy$. $F_{i,j}(u)$ and $G_{i,j}(u)$ are the integra average values for the fluxes $f(u)$ and $g(u)$ over $I_{i,j}$ as $\frac{1}{\Delta x\Delta y}\int_{I_{i,j}} f(u)dxdy$ and $\frac{1}{\Delta x\Delta y}\int_{I_{i,j}} g(u)dxdy$, respectively. $\hat{f}\left(u(x_{i+1/2},y)\right)$ and $\hat{g}\left(u(x,y_{j+1/2})\right)$ are the numerical fluxes to approximate the values of $f\left(u(x_{i+1/2},y,t)\right)$ and $g\left(u(x,y_{j+1/2},t)\right)$, respectively.

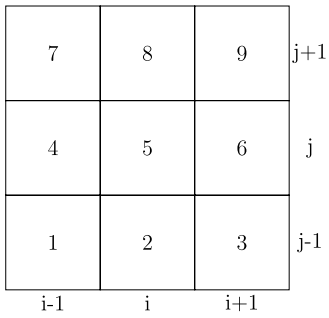

Fig. 2.1. The big stencil S_0 and its new labels.

Now, we approximate the integral terms of equations (2.8) by 3-point Gaussian numerical integration. For example,

$$F_{i,j}(u) = \frac{1}{\Delta x \Delta y} \int_{I_{i,j}} f(u) dx dy \approx \sum_{k=1}^{3} \sum_{l=1}^{3} \omega_k \omega_l f(u(x_{G_k}, y_{G_l})),$$

$$\int_{y_{j-1/2}}^{y_{j+1/2}} \hat{f}(u(x_{i+1/2}, y)) dy \approx \Delta y \sum_{k=1}^{3} \omega_k \hat{f}(u(x_{i+1/2}, y_{G_k})),$$

in which $\omega_1 = \frac{5}{18}$, $\omega_2 = \frac{4}{9}$ and $\omega_3 = \frac{5}{18}$ are the quadrature weights, and the coordinates of the Gaussian points are

$$x_{G_1} = x_{i-\frac{\sqrt{15}}{10}},\ x_{G_2} = x_i,\ x_{G_3} = x_{i+\frac{\sqrt{15}}{10}};\quad y_{G_1} = y_{j-\frac{\sqrt{15}}{10}},\ y_{G_2} = y_j,\ y_{G_3} = y_{j+\frac{\sqrt{15}}{10}}.$$

The numerical fluxes at the interface points in each directions are approximated by the Lax-Friedrichs method:

$$\hat{f}(u(G_b)) = \frac{1}{2}[f(u^-(G_b)) + f(u^+(G_b))] - \frac{\alpha}{2}(u^+(G_b) - u^-(G_b)),$$

and

$$\hat{g}(u(G_b)) = \frac{1}{2}[g(u^-(G_b)) + g(u^+(G_b))] - \frac{\beta}{2}(u^+(G_b) - u^-(G_b)).$$

Here, $\alpha = \max_u |f'(u)|$, $\beta = \max_u |g'(u)|$, and G_b is the Gaussian point on the interface of the cell $I_{i,j}$.

Now, we first present the detailed spatial reconstruction for the semi-discrete scheme (2.8) in Steps 4 and 5, then, we introduce the methodology of time discretization in Step 6.

Step 4. Identify the troubled-cell and modify the first order moments in the troubled-cell.

We also use the KXRCF troubled-cell indicator [23] to identify the discontinuities, and the detailed implementation procedures for two dimensional problems had been introduced in the hybrid HWENO scheme [44].

If the cell $I_{i,j}$ is identified as a troubled cell, we would mark its neighbor cells as troubled cells too as [44], then, we modify the first order moments in the troubled cells as following description. We can modify the first order moments employing dimensional by dimensional manner. For example, we use these information $\overline{u}_{i-1,j}$, $\overline{u}_{i,j}$, $\overline{u}_{i+1,j}$, $\overline{v}_{i-1,j}$, $\overline{v}_{i+1,j}$ to modify $\overline{v}_{i,j}$, but employ $\overline{u}_{i,j-1}$, $\overline{u}_{i,j}$, $\overline{u}_{i,j+1}$, $\overline{w}_{i,j-1}$, $\overline{w}_{i,j+1}$ to reconstruct $\overline{w}_{i,j}$, and the procedures are the same as one dimensional case.

Step 5. Reconstruct the point values of the solutions u at the Gaussian points.

Based on the formula of the semi-discrete scheme (2.8), it means that we need to reconstruct the point values of $u^{\pm}(x_{i\mp 1/2}, y_{G_{1,2,3}})$, $u^{\pm}(x_{G_{1,2,3}}, y_{j\mp 1/2})$ and $u(x_{G_{1,2,3}}, y_{G_{1,2,3}})$ in the cell $I_{i,j}$. If the cell $I_{i,j}$ is identified as a troubled cell in Step 4, we would reconstruct the points values of solutions u at the interface points of the cell $I_{i,j}$ by the HWENO methodology in Step 5.1; otherwise we directly use linear approximation at these interface points in Step 5.2. And we employ linear approximation straightforwardly for internal reconstructed points introduced in Step 5.3.

Step 5.1. Reconstruct the point values of the solutions u at the interface points by a new HWENO methodology.

If the cell $I_{i,j}$ is identified as a troubled cell, the points values of solutions u at the interface points of the cell $I_{i,j}$ are reconstructed by the next new HWENO methodology. We first give the big stencil S_0 in Fig. 2.1, and we rebel the cell $I_{i,j}$ and its neighboring cells as $I_1, ..., I_9$ for simplicity. Particularly, the new label of the cell $I_{i,j}$ is I_5. In the next procedures, we take G_k to represent the specific points where we want to reconstruct. We also give four small stencils $S_1, ..., S_4$ shown in Fig. 2.2. Notice that we only use five candidate stencils, but the hybrid HWENO scheme [44] needed to use eight small stencils. Now, we construct a quartic reconstruction polynomial $p_0(x, y) \in span\{1, x, y, x^2, xy, y^2, x^3, x^2y, xy^2, y^3, x^4, x^3y, x^2y^2, xy^3, y^4\}$ on the big stencil S_0 and four quadratic polynomials

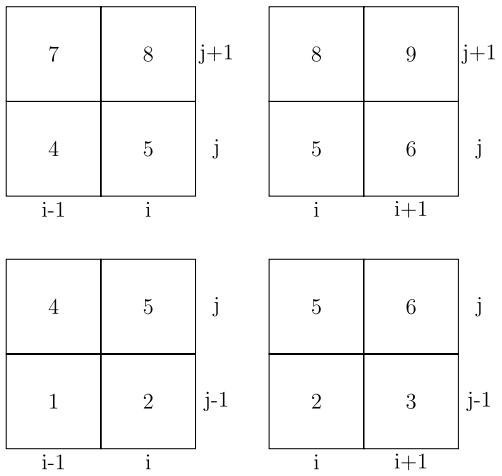

Fig. 2.2. The four small stencils and these respective labels. From left to right and bottom to top are the stencils: $S_1, ..., S_4$.

$p_1(x, y), ..., p_4(x, y) \in span\{1, x, y, x^2, xy, y^2\}$ on the four small stencils $S_1, ..., S_4$, respectively. These polynomials satisfy the following conditions:

$$\frac{1}{\Delta x\Delta y}\int_{I_k} p_n(x, y)dxdy = \overline{u}_k,$$
$$\frac{1}{\Delta x\Delta y}\int_{I_{k_x}} p_n(x, y)\frac{(x-x_{k_x})}{\Delta x}dxdy = \overline{v}_{k_x}, \quad \frac{1}{\Delta x\Delta y}\int_{I_{k_y}} p_n(x, y)\frac{(y-y_{k_y})}{\Delta y}dxdy = \overline{w}_{k_y},$$

for

$$n = 0, \quad k = 1, ..., 9, \ k_x = k_y = 2, 4, 5, 6, 8;$$
$$n = 1, \quad k = 1, 2, 4, 5, \ k_x = k_y = 5; \quad n = 2, \quad k = 2, 3, 5, 6, \ k_x = k_y = 5;$$
$$n = 3, \quad k = 4, 5, 7, 8, \ k_x = k_y = 5; \quad n = 4, \quad k = 5, 6, 8, 9, \ k_x = k_y = 5.$$

For the quartic polynomial $p_0(x, y)$, we can obtain it by requiring that it matches the zeroth order moments on the cell $I_1, ..., I_9$, the first order moments on the cell I_5 and others are in a least square sense [21]. For the four quadratic polynomials, we can directly obtain the expressions of $p_n(x, y)$ $(n = 1, ..., 4)$ by the above corresponding requirements, respectively.

Similarly as in the one dimensional case, the new HWENO method can use any artificial positive linear weights (the sum equals 1), while the hybrid HWENO scheme [44] needed to calculate the linear weights for 12 points using 8 small stencils determined by a least square methodology, and the linear weights were not easy to be obtained especially for high dimensional problems or unstructured meshes. In addition, it only had the fourth order accuracy in two dimension, but the new HWENO methodology can achieve the fifth order numerical accuracy. Next, to measure how smooth the function $p_n(x, y)$ in the target cell $I_{i,j}$, we compute the smoothness indicators β_n as the same way listed by [21], following as

$$\beta_n = \sum_{|l|=1}^{r} |I_{i,j}|^{|l|-1} \int_{I_{i,j}} \left(\frac{\partial^{|l|}}{\partial x^{l_1}\partial y^{l_2}} p_n(x, y)\right)^2 dxdy, \quad n = 0, ..., 4, \tag{2.9}$$

where $l = (l_1, l_2)$, $|l| = l_1 + l_2$ and r is the degree of $p_n(x, y)$. Similarly, we bring a new parameter τ to define the overall difference between β_l, $l = 0, ..., 4$ as

$$\tau = \left(\frac{|\beta_0 - \beta_1| + |\beta_0 - \beta_2| + |\beta_0 - \beta_3| + |\beta_0 - \beta_4|}{4}\right)^2, \tag{2.10}$$

then, the nonlinear weights are defined as

$$\omega_n = \frac{\bar{\omega}_n}{\sum_{\ell=0}^{4}\bar{\omega}_\ell}, \ \text{with } \bar{\omega}_n = \gamma_n(1 + \frac{\tau}{\beta_n + \varepsilon}), \ n = 0, ..., 4, \tag{2.11}$$

in which ε is taken as 10^{-6}. The final reconstruction of the solutions u at the interface point G_k is

$$u^*(G_k) = \omega_0\left(\frac{1}{\gamma_0}p_0(G_k) - \sum_{n=1}^{4}\frac{\gamma_n}{\gamma_0}p_n(G_k)\right) + \sum_{n=1}^{4}\omega_n p_n(G_k),$$

where "$*$" is "$+$" when G_k is located on the left or bottom interface of the cell $I_{i,j}$, while "$*$" is "$-$" on the right or top interface of $I_{i,j}$.

Step 5.2. Reconstruct the point values of the solutions u at the interface points using linear approximation.

If the cell $I_{i,j}$ is not identified as a troubled cell, the point value of the solution u at the interface point G_k is directly approximated by $p_0(G_k)$, and we use the same polynomial $p_0(x, y)$ given in Step 5.1.

Step 5.3. Reconstruct the point values of the solutions u at the internal points by linear approximation straightforwardly.

We would use linear approximation for the point values of the solutions u at the internal points in all cells, then, we directly employ the same quartic polynomial $p_0(x, y)$ obtained in Step 5.1 to approximate these point values.

Step 6. Discretize the semi-discrete scheme (2.8) in time by the third order TVD Runge-Kutta method [38].

The semi-discrete scheme (2.8) is discretized by the third order TVD Runge-Kutta method in time, and the formula is given in (2.6) for the one dimensional case.

Remark 3. The KXRCF indicator is suitable for two dimensional hyperbolic conservation laws. For two dimensional scalar equation, the solution u is the indicator variable. $\overrightarrow{v}$ is set as $f'(u)$ in the x direction, while it is taken as $g'(u)$ in the y direction. For two dimensional Euler equations, the density ρ and the energy E are defined as the indicator variables, respectively. $\overrightarrow{v}$ is the velocity μ in the x direction of the fluid, while it is the velocity ν in the y direction.

Remark 4. For the systems, such as the two dimensional compressible Euler equations, all HWENO reconstruction procedures are performed on the local characteristic decompositions, while linear approximation procedures are performed on component by component.

3. Numerical tests

In this section, we present the numerical results of the new hybrid HWENO scheme which is described in Section 2. In order to fully assess the influence of the modification of the first order moment upon accuracy, all cells are marked as troubled-cells in Step 1 and Step 4 for one and two dimensional cases, respectively, and we denote this method as New HWENO scheme. We also denote HWENO scheme and the hybrid HWENO scheme which are presented in [44]. In addition, we present the numerical results of the classical fifth order WENO schemes in the accuracy tests for comparison, and the schemes were introduced in [22] and [36] for one and two dimensional problems, respectively. The CFL number is set as 0.6 expect for the hybrid HWENO scheme in the two dimensional non-smooth tests.

3.1. Accuracy tests

We will present the results of HWENO, New HWENO, Hybrid HWENO, New hybrid HWENO and WENO schemes in the one and two dimensional accuracy tests. In addition, to evaluate whether the choice of the linear weights would affect the order of the new HWENO methodology or not, we use random positive linear weights (the sum equals one) at each time step for New HWENO and New hybrid HWENO schemes. Moreover, to survey the effect of the mesh for the accuracy, we would also present the numerical results of New HWENO scheme on non-uniform meshes in one dimensional accuracy tests for simplicity, and the non-uniform meshes are obtained by making the interface points of the uniform meshes to move 0-20% length randomly.

Example 3.1. We solve the following scalar Burgers' equation:

$$u_t + (\frac{u^2}{2})_x = 0, \quad 0 < x < 2. \tag{3.1}$$

The initial condition is $u(x, 0) = 0.5 + \sin(\pi x)$ with periodic boundary condition. The computing time is $t = 0.5/\pi$, in which the solution is still smooth. We give the numerical errors and orders in Table 3.1 with N uniform meshes for HWENO, New HWENO, Hybrid HWENO, New hybrid HWENO and WENO schemes. At first, we know that Hybrid HWENO and New hybrid HWENO schemes have same results for there are not cells which are identified as troubled-cells, therefore, they both directly use linear approximation for the spatial reconstruction. Although these HWENO and WENO schemes all have the designed fifth order accuracy, HWENO schemes have smaller numerical errors than WENO scheme starting with 80 cells, and the hybrid schemes have better numerical performances with smaller numerical errors than the corresponding HWENO schemes, meanwhile, we can see that New HWENO scheme has smaller numerical errors than HWENO scheme starting with 80 cells, which illustrates the new HWENO methodology has better numerical performance than the original HWENO method. In addition, the choice of the linear weights would not affect the order of the new HWENO methodology. We also find New HWENO scheme has the fifth order accuracy on the non-uniform meshes, which illustrates the new HWENO methodology is not particularly dependent on the meshes, and we don't need to calculate the linear weights in this case. Finally, we show numerical errors against CPU times by these HWENO and WENO schemes on the uniform meshes in Fig. 3.1, which shows two hybrid HWENO schemes have much higher efficiency than other HWENO schemes, and New HWENO scheme also has higher efficiency than HWENO scheme. New hybrid HWENO scheme also has higher efficiency than WENO scheme with smaller numerical errors and less computational time.

Table 3.1
1D-Burgers' equation: initial data $u(x,0) = 0.5 + sin(\pi x)$. HWENO and WENO schemes. $T = 0.5/\pi$. L^1 and L^∞ errors and orders.

Uniform meshes	HWENO scheme				New HWENO scheme			
	L^1 error	Order	L^∞ error	Order	L^1 error	Order	L^∞ error	Order
40	4.23E-05		5.25E-04		6.42E-04		6.89E-03	
80	1.24E-06	5.09	1.70E-05	4.95	4.20E-07	10.58	4.91E-06	10.45
120	1.72E-07	4.88	2.08E-06	5.17	3.97E-08	5.82	6.04E-07	5.17
160	4.26E-08	4.85	4.84E-07	5.08	8.83E-09	5.23	1.40E-07	5.08
200	1.34E-08	5.17	1.72E-07	4.64	2.80E-09	5.15	4.47E-08	5.12
240	5.21E-09	5.20	7.22E-08	4.76	1.10E-09	5.14	1.75E-08	5.16

Uniform meshes	Hybrid HWENO scheme				New Hybrid HWENO scheme			
	L^1 error	Order	L^∞ error	Order	L^1 error	Order	L^∞ error	Order
40	8.51E-07		1.14E-05		8.51E-07		1.14E-05	
80	1.46E-08	5.87	2.26E-07	5.65	1.46E-08	5.87	2.26E-07	5.65
120	1.39E-09	5.80	2.04E-08	5.94	1.39E-09	5.80	2.04E-08	5.94
160	2.66E-10	5.75	3.59E-09	6.03	2.66E-10	5.75	3.59E-09	6.03
200	7.46E-11	5.70	9.58E-10	5.92	7.46E-11	5.70	9.58E-10	5.92
240	2.68E-11	5.62	3.27E-10	5.90	2.68E-11	5.62	3.27E-10	5.90

Uniform meshes	WENO scheme			
	L^1 error	Order	L^∞ error	Order
40	1.24E-04		1.04E-03	
80	4.42E-06	4.82	4.73E-05	4.46
120	6.52E-07	4.72	6.06E-06	5.07
160	1.64E-07	4.79	1.39E-06	5.12
200	5.43E-08	4.96	6.25E-07	3.58
240	2.15E-08	5.09	3.00E-07	4.02

Non-uniform meshes	New HWENO scheme			
	L^1 error	Order	L^∞ error	Order
40	5.95E-04		5.42E-03	
80	5.33E-07	10.13	5.12E-06	10.05
120	4.62E-08	6.03	7.71E-07	4.67
160	9.41E-09	5.53	1.79E-07	5.07
200	3.17E-09	4.88	5.33E-08	5.43
240	1.17E-09	5.46	2.39E-08	4.40

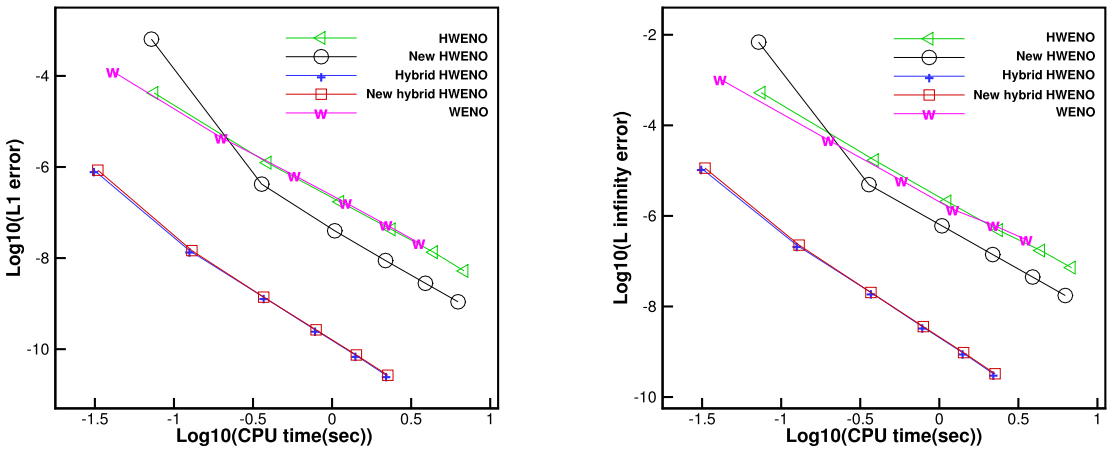

Fig. 3.1. 1D-Burgers' equation: initial data $u(x,0) = 0.5 + sin(\pi x)$. $T = 0.5/\pi$. Computing times and errors. Triangle signs and a green solid line: the results of HWENO scheme; circle signs and a black solid line: the results of New HWENO scheme; plus signs and a blue solid line: the results of Hybrid HWENO scheme; rectangle signs and a red solid line: the results of New hybrid HWENO scheme; "w" signs and a purple line: the results of WENO scheme. Uniform meshes. (For interpretation of the colors in the figure(s), the reader is referred to the web version of this article.)

Table 3.2
1D-Euler equations: initial data $\rho(x,0) = 1 + 0.2\sin(\pi x)$, $\mu(x,0) = 1$ and $p(x,0) = 1$. HWENO and WENO schemes. $T = 2$. L^1 and L^∞ errors and orders.

Uniform meshes	HWENO scheme				New HWENO scheme			
	L^1 error	Order	L^∞ error	Order	L^1 error	Order	L^∞ error	Order
40	4.00E-06		8.18E-06		9.09E-07		4.85E-06	
80	1.22E-07	5.04	2.43E-07	5.08	7.89E-09	6.85	3.76E-08	7.01
120	1.59E-08	5.03	3.05E-08	5.11	1.04E-09	5.01	2.44E-09	6.75
160	3.73E-09	5.03	6.71E-09	5.26	2.46E-10	5.00	4.54E-10	5.84
200	1.21E-09	5.04	2.12E-09	5.17	8.05E-11	5.00	1.37E-10	5.37
240	4.82E-10	5.06	8.35E-10	5.10	3.23E-11	5.00	5.25E-11	5.26

Uniform meshes	Hybrid HWENO scheme				New hybrid HWENO scheme			
	L^1 error	Order	L^∞ error	Order	L^1 error	Order	L^∞ error	Order
40	1.02E-09		1.60E-09		1.02E-09		1.60E-09	
80	3.10E-11	5.05	4.86E-11	5.04	3.10E-11	5.05	4.86E-11	5.04
120	4.06E-12	5.01	6.37E-12	5.01	4.06E-12	5.01	6.37E-12	5.01
160	9.61E-13	5.01	1.51E-12	5.01	9.61E-13	5.01	1.51E-12	5.01
200	3.15E-13	5.00	4.94E-13	5.00	3.15E-13	5.00	4.94E-13	5.00
240	1.26E-13	5.00	1.98E-13	5.00	1.26E-13	5.00	1.98E-13	5.00

Uniform meshes	WENO scheme			
	L^1 error	Order	L^∞ error	Order
40	2.04E-05		3.72E-05	
80	6.45E-07	4.98	1.21E-06	4.94
120	8.49E-08	5.00	1.58E-07	5.03
160	2.01E-08	5.01	3.67E-08	5.07
200	6.55E-09	5.02	1.16E-08	5.17
240	2.61E-09	5.04	4.46E-09	5.25

Non-uniform meshes	HWENO scheme			
	L^1 error	Order	L^∞ error	Order
40	9.70E-07		5.21E-06	
80	7.95E-09	6.93	2.80E-08	7.54
120	1.05E-09	5.00	2.14E-09	6.35
160	2.49E-10	4.99	4.22E-10	5.64
200	8.01E-11	5.09	1.33E-10	5.18
240	3.33E-11	4.81	5.33E-11	5.01

Example 3.2. One dimensional Euler equations:

$$\frac{\partial}{\partial t}\begin{pmatrix}\rho\\ \rho\mu\\ E\end{pmatrix} + \frac{\partial}{\partial x}\begin{pmatrix}\rho\mu\\ \rho\mu^2 + p\\ \mu(E+p)\end{pmatrix} = 0, \tag{3.2}$$

where ρ is density, μ is velocity, E is total energy and p is pressure. The initial conditions are $\rho(x,0) = 1 + 0.2\sin(\pi x)$, $\mu(x,0) = 1$, $p(x,0) = 1$ and $\gamma = 1.4$ with periodic boundary condition. The computing domain is $x \in [0, 2\pi]$. The exact solution is $\rho(x,t) = 1 + 0.2\sin(\pi(x-t))$, $\mu(x,0) = 1$, $p(x,0) = 1$, and the computing time is up to $T = 2$. We present the numerical errors and orders of the density for the HWENO and WENO schemes in Table 3.2, then, we first can see these HWENO and WENO schemes achieve the fifth order accuracy, but HWENO schemes have smaller numerical errors with more compact spatial stencil, and two hybrid HWENO schemes have same performances as they both directly use linear approximation for the spatial reconstruction, meanwhile, the hybrid schemes have smaller numerical errors than the corresponding HWENO schemes. In addition, New HWENO scheme has smaller numerical errors than HWENO scheme, which shows the new HWENO methodology has better performance than the original HWENO method, and random positive linear weights at each time step would not affect the order accuracy of New HWENO scheme. We also can see New HWENO scheme has the fifth order accuracy on the non-uniform meshes, and any random positive linear weights (the sum equals one) can be used, while the HWENO scheme [44] must calculate the linear weights in advance, and the linear weights wouldn't be easily obtained especially for the non-uniform meshes. Finally, we give the numerical errors against CPU times by these HWENO and WENO schemes on the uniform meshes in Fig. 3.2, which shows Hybrid HWENO schemes have much higher efficiency with smaller numerical errors and less CPU times than other HWENO schemes, and we can see New HWENO scheme has higher efficiency with smaller errors than HWENO scheme. In addition, all HWENO schemes have higher efficiency than WENO scheme with smaller numerical errors.

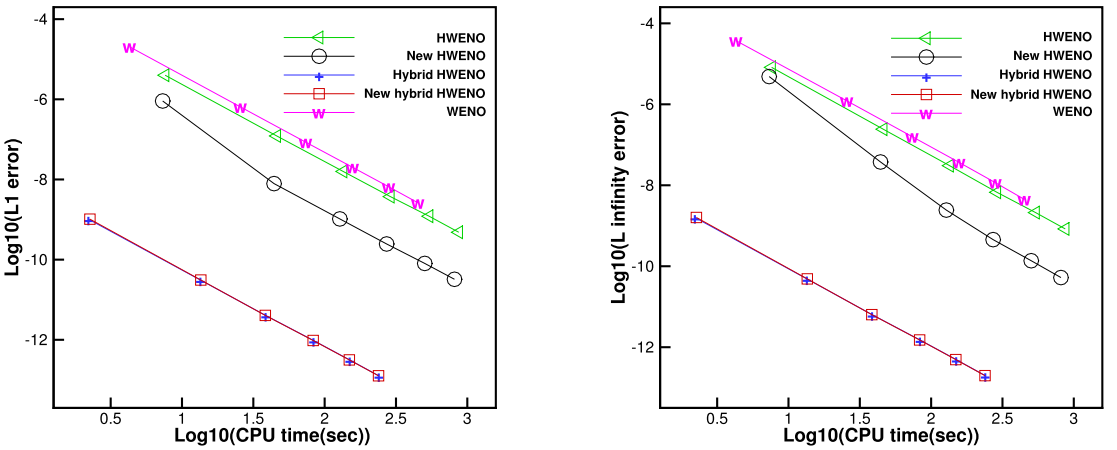

Fig. 3.2. 1D-Euler equations: initial data $\rho(x,0) = 1 + 0.2\sin(\pi x)$, $\mu(x,0) = 1$ and $p(x,0) = 1$. $T = 2$. Computing times and errors. Triangle signs and a green solid line: the results of HWENO scheme; circle signs and a black solid line: the results of New HWENO scheme; plus signs and a blue solid line: the results of Hybrid HWENO scheme; rectangle signs and a red solid line: the results of New hybrid HWENO scheme; "w" signs and a purple line: the results of WENO scheme. Uniform meshes.

Table 3.3
2D-Burgers' equation: initial data $u(x,y,0) = 0.5 + sin(\pi(x+y)/2)$. HWENO and WENO schemes. $T = 0.5/\pi$. L^1 and L^∞ errors and orders. Uniform meshes with $N_x \times N_y$ cells.

$N_x \times N_y$ cells	HWENO scheme				New HWENO scheme			
	L^1 error	Order	L^∞ error	Order	L^1 error	Order	L^∞ error	Order
40×40	8.21E-05		7.02E-04		1.28E-04		1.10E-03	
80×80	4.67E-06	4.14	4.42E-05	3.99	2.86E-07	8.81	2.25E-06	8.94
120×120	8.70E-07	4.15	7.76E-06	4.29	2.52E-08	5.99	3.04E-07	4.95
160×160	2.66E-07	4.13	2.26E-06	4.29	5.60E-09	5.22	7.19E-08	5.00
200×200	1.06E-07	4.12	8.73E-07	4.26	1.79E-09	5.12	2.39E-08	4.95
240×240	5.02E-08	4.09	4.04E-07	4.23	7.12E-10	5.05	9.53E-09	5.03

$N_x \times N_y$ cells	Hybrid HWENO scheme				New Hybrid HWENO scheme			
	L^1 error	Order	L^∞ error	Order	L^1 error	Order	L^∞ error	Order
40×40	7.03E-05		6.32E-04		2.70E-06		2.49E-05	
80×80	3.93E-06	4.16	4.28E-05	3.88	5.01E-08	5.75	8.91E-07	4.81
120×120	7.27E-07	4.16	7.61E-06	4.26	4.15E-09	6.14	7.81E-08	6.00
160×160	2.18E-07	4.19	2.30E-06	4.16	7.00E-10	6.18	1.27E-08	6.32
200×200	8.61E-08	4.16	8.95E-07	4.23	1.94E-10	5.74	3.26E-09	6.09
240×240	4.05E-08	4.14	4.18E-07	4.18	7.65E-11	5.12	1.17E-09	5.63

$N_x \times N_y$ cells	WENO scheme			
	L^1 error	Order	L^∞ error	Order
40×40	8.21E-05		6.74E-04	
80×80	4.06E-06	4.34	3.91E-05	4.11
120×120	6.29E-07	4.60	5.67E-06	4.76
160×160	1.66E-07	4.64	1.42E-06	4.81
200×200	5.64E-08	4.82	4.96E-07	4.71
240×240	2.27E-08	4.99	2.23E-07	4.40

Example 3.3. Two dimensional Burgers' equation:

$$u_t + (\frac{u^2}{2})_x + (\frac{u^2}{2})_y = 0, \quad 0 < x < 4,\ 0 < y < 4. \tag{3.3}$$

The initial condition is $u(x,y,0) = 0.5 + sin(\pi(x+y)/2)$ and periodic boundary conditions are applied in each direction. We compute the solution up to $T = 0.5/\pi$, where the solution is smooth, and we present the numerical errors and orders of HWENO and WENO schemes in Table 3.3, which illustrates that New HWENO, New hybrid HWENO and WENO schemes have the fifth order accuracy, and the HWENO and hybrid HWENO schemes only have the fourth order accuracy, but all HWENO schemes are more compact for only using the immediate neighbor information. We also can see that different choice of the linear weights has no influence on the numerical accuracy for the new HWENO methodology. In addition,

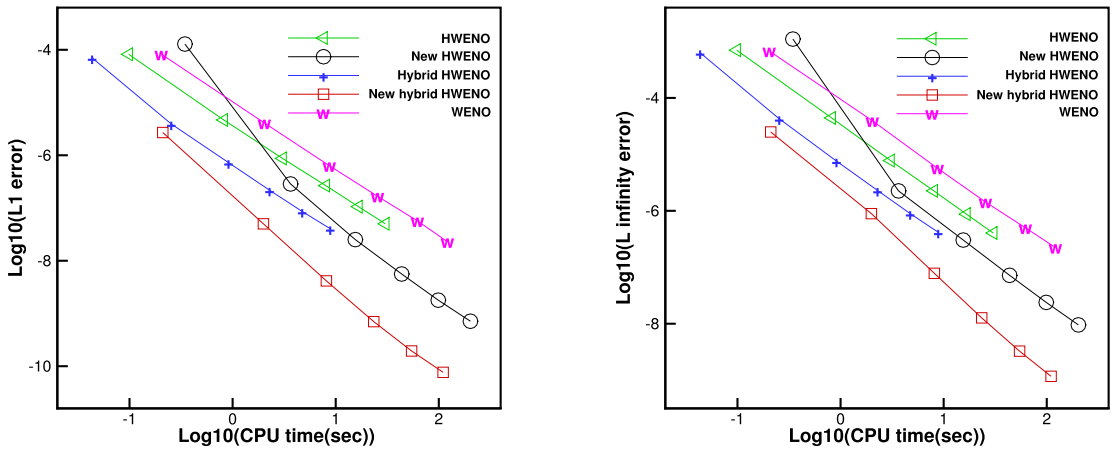

Fig. 3.3. 2D-Burgers' equation: initial data $u(x, y, 0) = 0.5 + sin(\pi(x + y)/2)$. $T = 0.5/\pi$. Computing times and errors. Triangle signs and a green solid line: the results of HWENO scheme; circle signs and a black solid line: the results of New HWENO scheme; plus signs and a blue solid line: the results of Hybrid HWENO scheme; rectangle signs and a red solid line: the results of New hybrid HWENO scheme; "w" signs and a purple line: the results of WENO scheme. Uniform meshes.

Table 3.4
2D-Euler equations: initial data $\rho(x, y, 0) = 1 + 0.2\sin(\pi(x + y))$, $\mu(x, y, 0) = 1$, $\nu(x, y, 0) = 1$ and $p(x, y, 0) = 1$. HWENO and WENO schemes. $T = 2$. L^1 and L^∞ errors and orders. Uniform meshes with $N_x \times N_y$ cells.

$N_x \times N_y$ cells	HWENO scheme				New HWENO scheme			
	L^1 error	Order	L^∞ error	Order	L^1 error	Order	L^∞ error	Order
30×30	8.85E-05		1.63E-04		6.78E-06		2.86E-05	
60×60	4.39E-06	4.33	7.09E-06	4.52	6.64E-08	6.67	2.71E-07	6.72
90×90	8.08E-07	4.17	1.29E-06	4.20	8.73E-09	5.00	2.04E-08	6.38
120×120	2.48E-07	4.11	3.95E-07	4.11	2.07E-09	5.00	3.88E-09	5.77
150×150	1.00E-07	4.07	1.59E-07	4.07	6.78E-10	5.00	1.14E-09	5.48
180×180	4.77E-08	4.05	7.59E-08	4.05	2.72E-10	5.00	4.44E-10	5.18

$N_x \times N_y$ cells	Hybrid HWENO scheme				New hybrid HWENO scheme			
	L^1 error	Order	L^∞ error	Order	L^1 error	Order	L^∞ error	Order
30×30	2.37E-05		3.72E-05		3.11E-07		4.87E-07	
60×60	7.76E-07	4.93	1.22E-06	4.93	4.55E-09	6.09	7.14E-09	6.09
90×90	1.07E-07	4.89	1.68E-07	4.89	3.95E-10	6.03	6.20E-10	6.03
120×120	2.67E-08	4.82	4.20E-08	4.82	7.01E-11	6.01	1.10E-10	6.00
150×150	9.27E-09	4.75	1.46E-08	4.75	1.84E-11	5.99	3.00E-11	5.84
180×180	3.95E-09	4.68	6.21E-09	4.67	6.19E-12	5.98	9.71E-12	5.98

$N_x \times N_y$ cells	WENO scheme			
	L^1 error	Order	L^∞ error	Order
30×30	2.45E-05		4.70E-05	
60×60	5.57E-07	5.46	1.40E-06	5.07
90×90	6.29E-08	5.38	1.76E-07	5.11
120×120	1.38E-08	5.26	3.79E-08	5.34
150×150	4.31E-09	5.23	1.09E-08	5.58
180×180	1.68E-09	5.16	3.77E-09	5.83

we present the numerical errors against CPU times by these HWENO and WENO schemes in Fig. 3.3, which illustrates New hybrid HWENO scheme has higher efficiency than Hybrid HWENO scheme with smaller numerical errors and higher order numerical accuracy, and the hybrid schemes both have less CPU times than the corresponding schemes. Meanwhile, New HWENO scheme has higher efficiency than HWENO scheme, and all HWENO schemes have higher efficiency than WENO scheme.

Example 3.4. Two dimensional Euler equations:

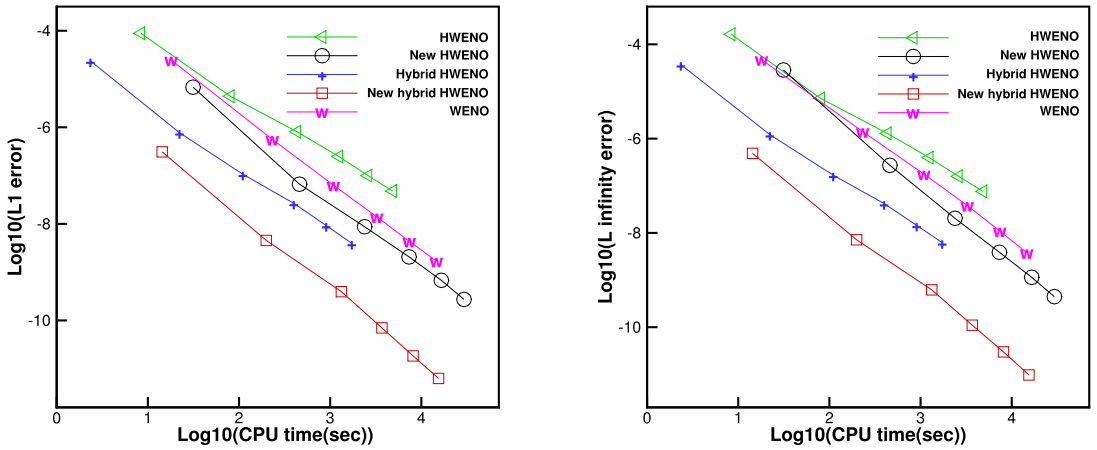

Fig. 3.4. 2D-Euler equations: initial data $\rho(x, y, 0) = 1 + 0.2\sin(\pi(x + y))$, $\mu(x, y, 0) = 1$, $\nu(x, y, 0) = 1$ and $p(x, y, 0) = 1$. $T = 2$. Computing times and errors. Triangle signs and a green solid line: the results of HWENO scheme; circle signs and a black solid line: the results of New HWENO scheme; plus signs and a blue solid line: the results of Hybrid HWENO scheme; rectangle signs and a red solid line: the results of New hybrid HWENO scheme; "w" signs and a purple line: the results of WENO scheme. Uniform meshes.

$$\frac{\partial}{\partial t}\begin{pmatrix}\rho\\ \rho\mu\\ \rho\nu\\ E\end{pmatrix}+\frac{\partial}{\partial x}\begin{pmatrix}\rho\mu\\ \rho\mu^2+p\\ \rho\mu\nu\\ \mu(E+p)\end{pmatrix}+\frac{\partial}{\partial y}\begin{pmatrix}\rho\nu\\ \rho\mu\nu\\ \rho\nu^2+p\\ \nu(E+p)\end{pmatrix}=0, \tag{3.4}$$

in which ρ is the density; (μ, ν) is the velocity; E is the total energy; and p the is pressure. The initial conditions are $\rho(x, y, 0) = 1 + 0.2\sin(\pi(x + y))$, $\mu(x, y, 0) = 1$, $\nu(x, y, 0) = 1$, $p(x, y, 0) = 1$ and $\gamma = 1.4$. The computing domain is $(x, y) \in [0, 2] \times [0, 2]$ with periodic boundary conditions in x and y directions, respectively. The exact solution of ρ is $\rho(x, y, t) = 1 + 0.2\sin(\pi(x + y - 2t))$ and the computing time is $T = 2$. We give the numerical errors and orders of the density for HWENO, New HWENO, Hybrid HWENO, New hybrid HWENO and WENO schemes in Table 3.4, then, we can find the New HWENO, New hybrid HWENO and WENO schemes achieve the fifth order accuracy, and the HWENO and Hybrid HWENO scheme only have the fourth order accuracy. However, HWENO schemes use more compact spatial reconstructed stencil than WENO scheme. Meanwhile, we can see that random positive linear weights (the sum equals one) would have no impact on the order accuracy of New HWENO scheme. Finally, we also show their numerical errors against CPU times in Fig. 3.4, which illustrates New hybrid HWENO scheme has higher efficiency than other four schemes, meanwhile, New HWENO scheme has better performance with less numerical errors and higher order accuracy than HWENO scheme. In addition, New HWENO and New Hybrid HWENO schemes have higher efficiency than WENO scheme with smaller numerical errors.

3.2. Non-smooth tests

We present the results of the new hybrid HWENO scheme here, meanwhile, the linear weights for the low degree polynomials are set as 0.01 and the linear weight for the high degree polynomial is the rest (the sum of their linear weights equals one), and we also show the performance of the new hybrid HWENO scheme with random positive linear weights on the uniform meshes in one dimensional non-smooth tests. In addition, we present the numerical results of the new hybrid HWENO scheme with fixed and random positive linear weights on the non-uniform meshes for one dimensional problems, and the non-uniform meshes are obtained by the same way as the one dimensional accuracy tests. For comparison, we also present the numerical results of the hybrid HWENO scheme [44]. From the results of the non-smooth tests, two schemes have similar performances in one dimension, but the new hybrid HWENO scheme has better numerical performances in two dimension for the new hybrid HWENO scheme has higher order numerical accuracy. In addition, the new hybrid HWENO scheme uses more simpler HWENO methodology, where any artificial positive linear weights (the sum equals 1) can be used, which is easier to implement in the computation, and it also uses less candidate stencils and bigger CFL number for two dimensional problems.

Example 3.5. We solve the one-dimensional Burgers' equation (3.1) as introduced in Example 3.1 with same initial and boundary conditions, but the final computing time is $t = 1.5/\pi$, in which the solution is discontinuous. In Fig. 3.5, we present the numerical solution of the HWENO schemes and the exact solution, and we can see that two schemes have similar numerical results with high resolutions. In addition, the performances are similar for the new hybrid HWENO scheme with fixed and random positive linear weights on the uniform and non-uniform meshes.

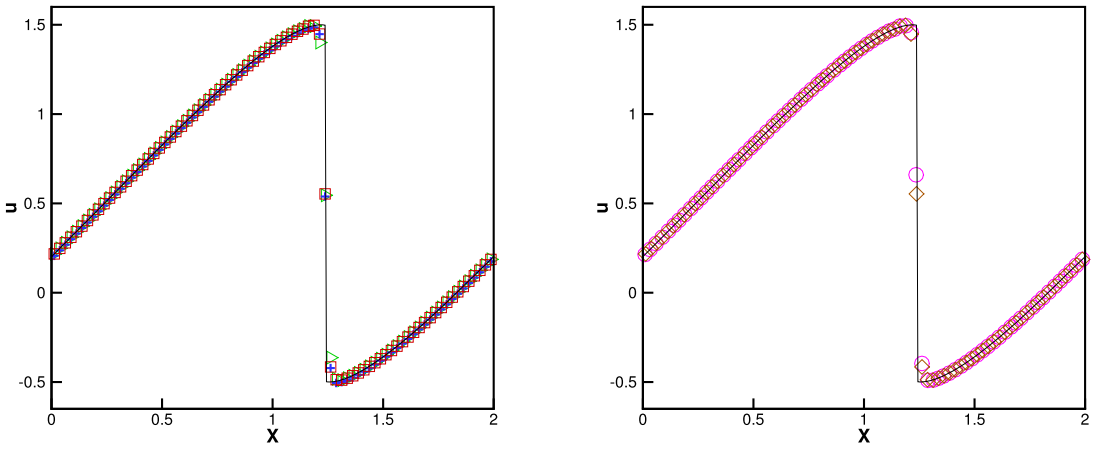

Fig. 3.5. 1D-Burgers' equation: initial data $u(x,0) = 0.5 + sin(\pi x)$. $T = 1.5/\pi$. From left to right: the results of HWENO schemes on the uniform and non-uniform meshes. Black solid line: exact solution; blue plus signs: the results of the hybrid HWENO scheme; red squares and purple circles: the results of the new hybrid HWENO scheme with fixed positive linear weights; green triangles and brown diamonds: the results of the new hybrid HWENO scheme with random positive linear weights. 80 cells.

Example 3.6. The Lax problem for 1D Euler equations with the next Riemann initial condition:

$$(\rho, \mu, p, \gamma)^T = \begin{cases} (0.445, 0.698, 3.528, 1.4)^T, & x \in [-0.5, 0), \\ (0.5, 0, 0.571, 1.4)^T, & x \in [0, 0.5]. \end{cases}$$

The computing time is $T = 0.16$. In Fig. 3.6, we plot the exact solution against the computed density ρ obtained with the HWENO schemes, the zoomed in picture and the time history of the cells where the modification procedure is used in the new hybrid HWENO scheme with fixed and random positive linear weights on the uniform and non-uniform meshes. We can first see the results computed by the new hybrid HWENO scheme with random positive linear weights on the uniform meshes is closer to the exact solution, and we also find that only 13.41% cells in this case where we use the new HWENO methodology, which means that most regions directly use linear approximation with no modification for the first order moments and no HWENO reconstruction for the spatial discretization. For the new hybrid HWENO scheme in other cases, similar cells are identified as the troubled cells, which shows the KXRCF troubled-cell indicator doesn't rely on the cells or the linear weights. The new hybrid HWENO scheme keeps good resolutions too, and the performances are also similar in this numerical test for the new hybrid HWENO scheme with fixed and random positive linear weights on the uniform and non-uniform meshes.

Example 3.7. The Shu-Osher problem, which has a shock interaction with entropy waves [36]. The initial condition is

$$(\rho, \mu, p, \gamma)^T = \begin{cases} (3.857143, 2.629369, 10.333333, 1.4)^T, & x \in [-5, -4), \\ (1 + 0.2\sin(5x), 0, 1, 1.4)^T, & x \in [-4, 5]. \end{cases}$$

This is a typical example both containing shocks and complex smooth region structures, which has a moving Mach=3 shock interacting with sine waves in density. The computing time is up to $T = 1.8$. In Fig. 3.7, we plot the computed density ρ by HWENO schemes against the referenced "exact" solution, the zoomed in picture and the time history of the troubled-cells for the new hybrid HWENO scheme with fixed and random positive linear weights on the uniform and non-uniform meshes. The referenced "exact" solution is computed by the fifth order finite difference WENO scheme [22] with 2000 grid points. We can see two schemes have similar numerical results with high resolutions, but the new hybrid HWENO scheme doesn't need to calculate the linear weights in advance. In addition, only 3.54% cells are identified as the troubled-cells where we need to modify their first order moments for the new hybrid HWENO scheme with the fixed linear weights on the uniform meshes, and similar cells are identified as the troubled-cells for the new hybrid HWENO scheme in other cases, which illustrates the KXRCF troubled-cell indicator is suitable for our scheme even though the cells or the linear weights are different. From Fig. 3.7, we first find the performances are similar for the original hybrid HWENO scheme and the new hybrid HWENO scheme on the uniform meshes with fixed linear weights. We also notice that the new hybrid scheme with fixed positive linear weights has better performance than the scheme with random positive linear weights. The reason may be that the linear weight of the high degree polynomial would be very small in some time steps for the scheme with random positive linear weights, and it means the reconstruction would use more information from the low degree polynomial, which would affect the performance especially for the test both containing shocks and complex smooth region structures.

Example 3.8. We solve the next interaction of two blast waves problem. The initial conditions are:

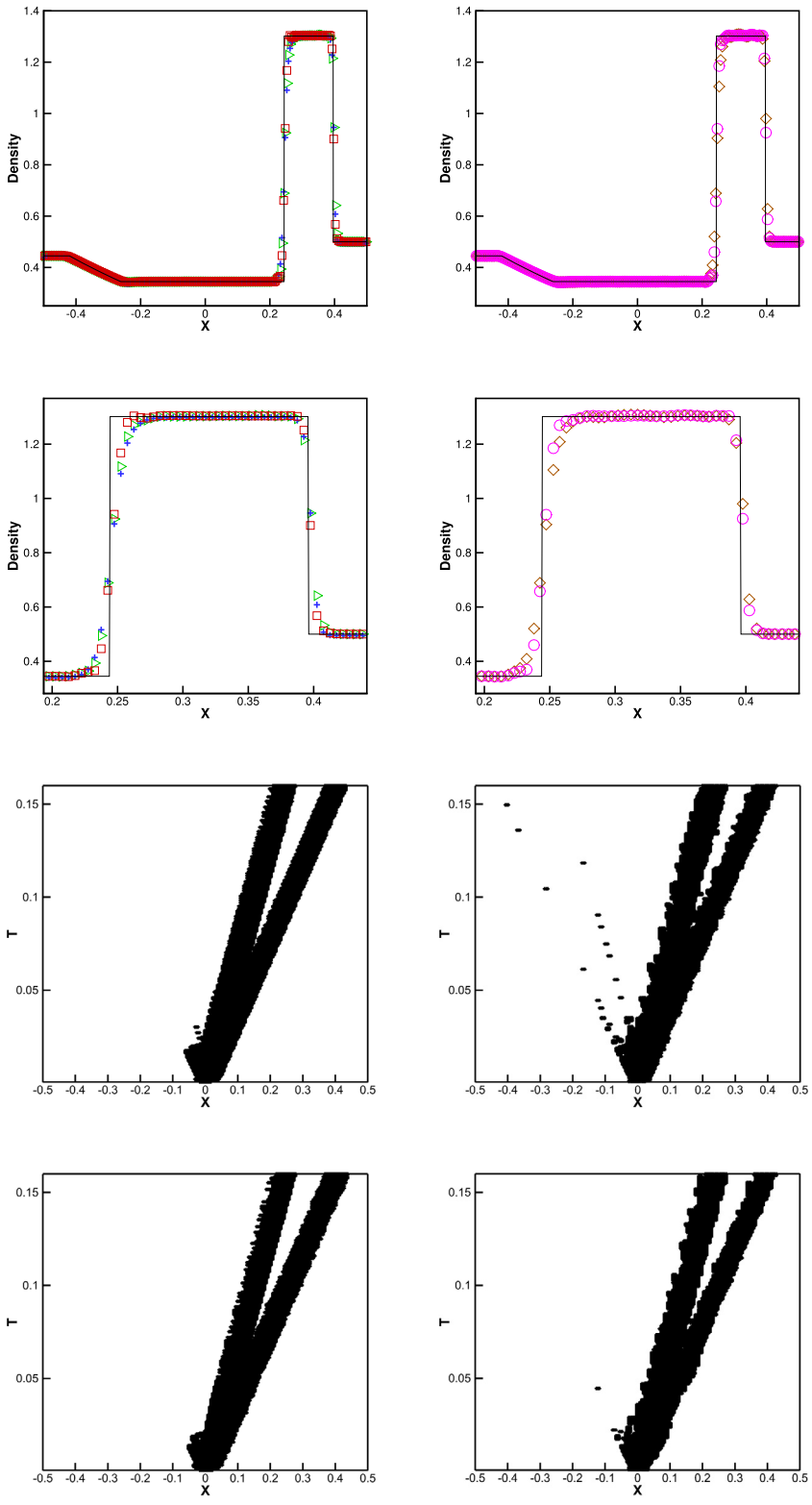

Fig. 3.6. The Lax problem. $T = 0.16$. From left to right: the results of HWENO schemes on the uniform and non-uniform meshes. From top to bottom: density; density zoomed in; the cells where the modification for the first order moments are computed in the new hybrid HWENO scheme with fixed and random positive linear weights. Black solid line: exact solution; blue plus signs: the results of the hybrid HWENO scheme; red squares and purple circles: the results of the new hybrid HWENO scheme with fixed positive linear weights; green triangles and brown diamonds: the results of the new hybrid HWENO scheme with random positive linear weights. 200 cells.

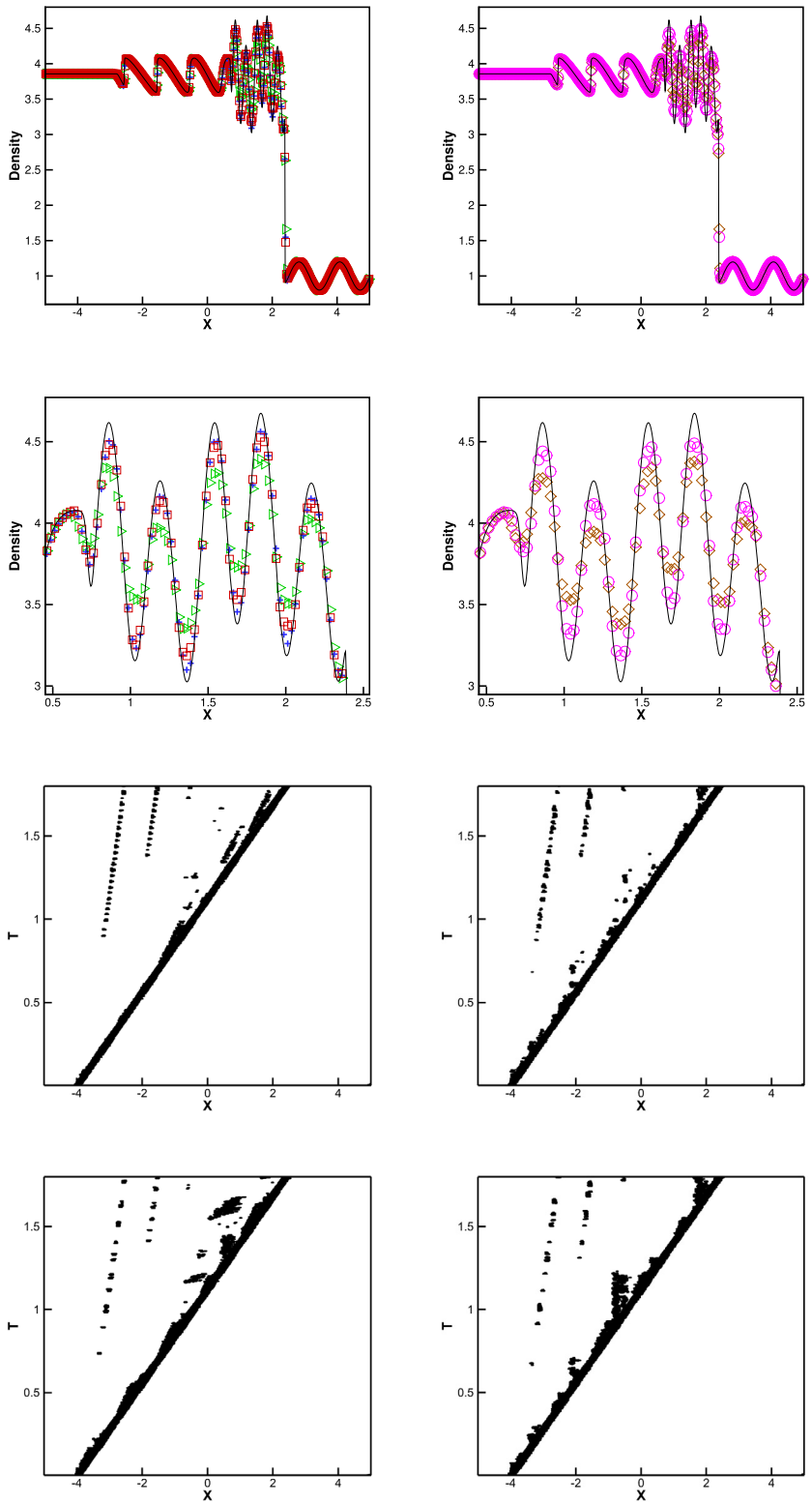

Fig. 3.7. The shock density wave interaction problem. $T = 1.8$. From left to right: the results of HWENO schemes on the uniform and non-uniform meshes. From top to bottom: density; density zoomed in; the cells where the modification for the first order moments are computed in the new hybrid HWENO scheme with fixed and random positive linear weights. Black solid line: exact solution; blue plus signs: the results of the hybrid HWENO scheme; red squares and purple circles: the results of the new hybrid HWENO scheme with fixed positive linear weights; green triangles and brown diamonds: the results of the new hybrid HWENO scheme with random positive linear weights. 400 cells.

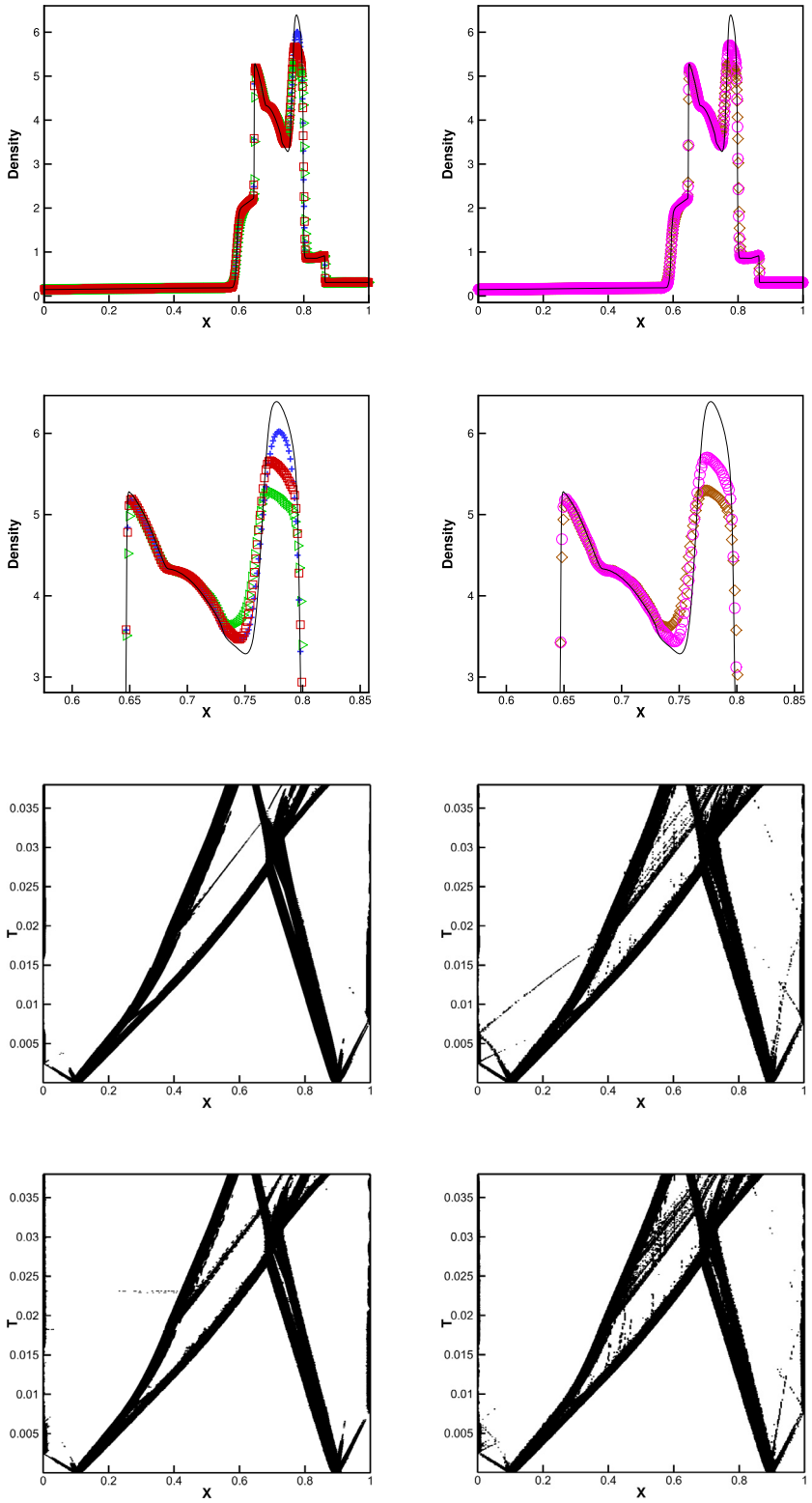

Fig. 3.8. The blast wave problem. $T = 0.038$. From left to right: the results of HWENO schemes on the uniform and non-uniform meshes. From top to bottom: density; density zoomed in; the cells where the modification for the first order moments are computed in the new hybrid HWENO scheme with fixed and random positive linear weights. Black solid line: exact solution; blue plus signs: the results of the hybrid HWENO scheme; red squares and purple circles: the results of the new hybrid HWENO scheme with fixed positive linear weights; green triangles and brown diamonds: the results of the new hybrid HWENO scheme with random positive linear weights. 800 cells.

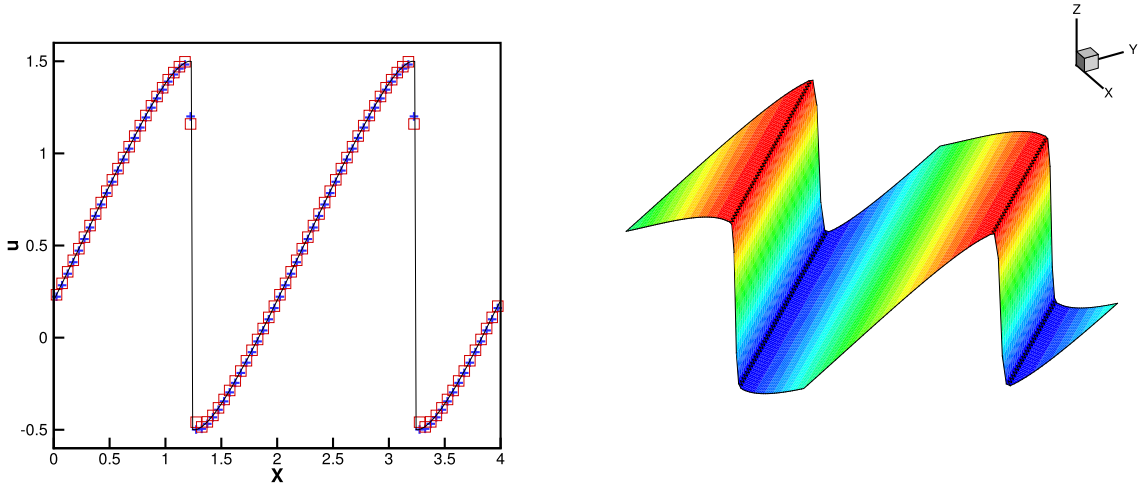

Fig. 3.9. 2D-Burgers' equation: initial data $u(x, y, 0) = 0.5 + sin(\pi(x + y)/2)$. $T = 1.5/\pi$. From left to right: the numerical solution at $x = y$ computed by HWENO schemes; the surface of the numerical solution for the new hybrid HWENO scheme. Black solid line: exact solution; blue plus signs: the results of the hybrid HWENO scheme; red squares: the results of the new hybrid HWENO scheme. Uniform meshes with 80×80 cells.

$$(\rho, \mu, p, \gamma)^T = \begin{cases} (1, 0, 10^3, 1.4)^T, & 0 < x < 0.1, \\ (1, 0, 10^{-2}, 1.4)^T, & 0.1 < x < 0.9, \\ (1, 0, 10^2, 1.4)^T, & 0.9 < x < 1. \end{cases}$$

The computing time is $T = 0.038$, and the reflective boundary condition is applied here. In Fig. 3.8, we also plot the computed density against the reference "exact" solution, the zoomed in picture and the time history of the troubled-cells for the new hybrid HWENO scheme with fixed and random positive linear weights on the uniform and non-uniform meshes. The reference "exact" solution is also computed by the fifth order finite difference WENO scheme [22] with 2000 grid points. We notice that the hybrid HWENO scheme has better performance than the new hybrid HWENO scheme with fixed positive linear weights on the uniform meshes. The reason maybe that the modification for the first order moments uses more information provided by the two linear polynomials in this example, but the new HWENO methodology is easy to implement in the computation. Similarly, only 13.94% cells are identified as the troubled-cells in this case, and we directly use high order linear approximation on other cells. Similar cells are identified as the troubled cells for the new hybrid HWENO scheme in other cases, which shows the cells or the linear weights wouldn't affect the ability of the KXRCF troubled-cell indicator. In addition, we also find the new hybrid scheme with fixed positive linear weights has better performance than the scheme with random positive linear weights as the Shu-Osher problem, and in practice, we recommend that the ratio between the linear weight of the high degree polynomial and the linear weights of the low degree polynomials is approximately 100 to 1.

Example 3.9. We solve the two-dimensional Burgers' equation (3.3) given in Example 3.3. The same initial and boundary conditions are applied here, but the computing time is up to $T = 1.5/\pi$, in which the solution is discontinuous. In Fig. 3.9, we present the numerical solution computed by HWENO schemes against the exact solution and the surface of the numerical solution by the new hybrid HWENO scheme. Similarly, we can see the HWENO schemes have high resolutions.

Example 3.10. We now solve double Mach reflection problem [42] modeled by the two-dimensional Euler equations (3.4). The computational domain is $[0, 4] \times [0, 1]$. The boundary conditions are: a reflection wall lies at the bottom from $x = \frac{1}{6}$, $y = 0$ with a 60^o angle based on x-axis. For the bottom boundary, the reflection boundary condition are applied, but the part from $x = 0$ to $x = \frac{1}{6}$ imposes the exact post-shock condition. For the top boundary, it is the exact motion of the Mach 10 shock. $\gamma = 1.4$ and the final computing time is up to $T = 0.2$. In Fig. 3.10, we plot the pictures of region $[0, 3] \times [0, 1]$, the locations of the troubled-cells at the final time and the blow-up region around the double Mach stems. The new hybrid HWENO scheme has better density resolutions than the hybrid HWENO scheme, in addition, the hybrid HWENO scheme needs to use smaller CFL number taken as 0.45, but the CFL number for the new hybrid HWENO scheme is 0.6, moreover, the new hybrid HWENO scheme uses less candidate stencils but has higher order numerical accuracy.

Example 3.11. We finally solve the problem of a Mach 3 wind tunnel with a step [42] modeled by the two-dimensional Euler equations (3.4). The wind tunnel is 1 length unit wide and 3 length units long. The step is 0.2 length units high and is located 0.6 length units from a right-going Mach 3 flow. Reflective boundary conditions are applied along the wall of the tunnel. In flow and out flow boundary conditions are applied at the entrance and the exit, respectively. The computing time

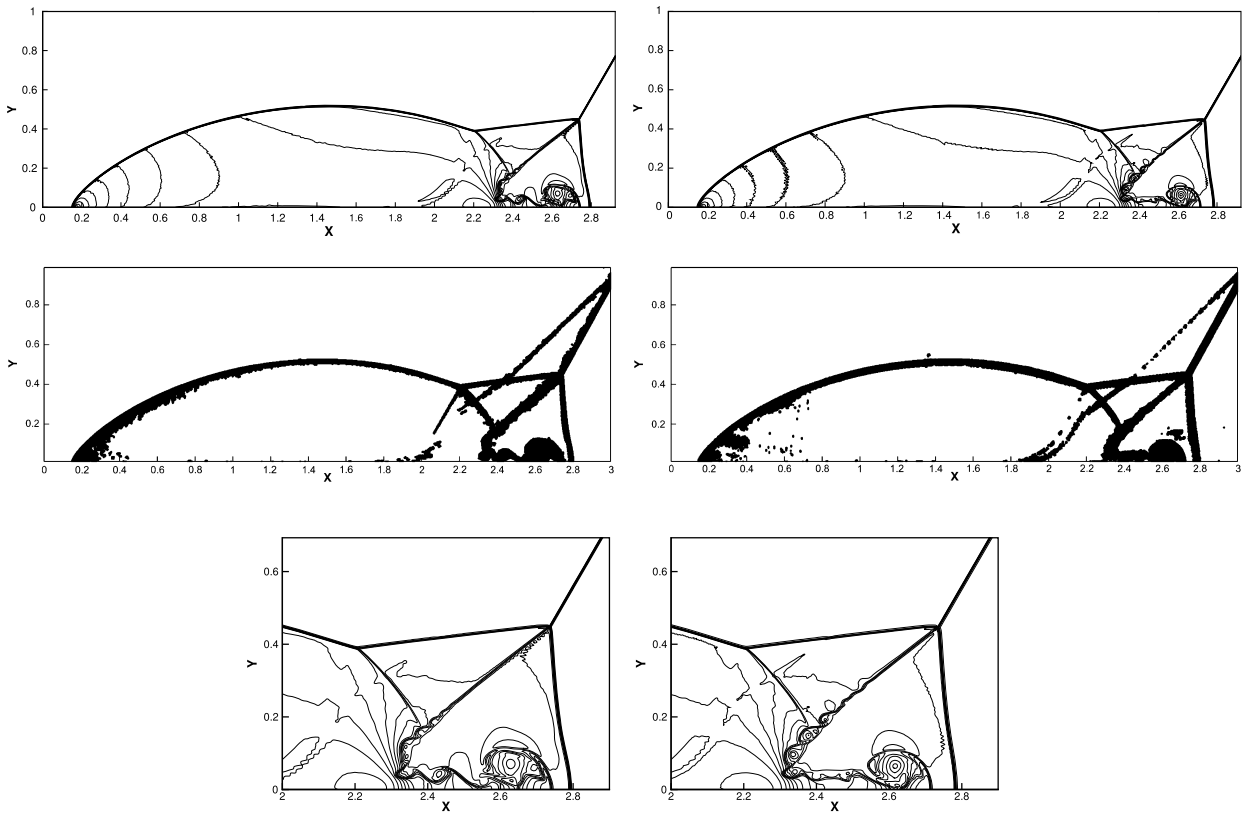

Fig. 3.10. Double Mach reflection problem. $T = 0.2$. From top to bottom: 30 equally spaced density contours from 1.5 to 22.7; the locations of the troubled-cells at the final time; zoom-in pictures around the Mach stem. The hybrid HWENO scheme (left); the new hybrid HWENO scheme (right). Uniform meshes with 1920×480 cells.

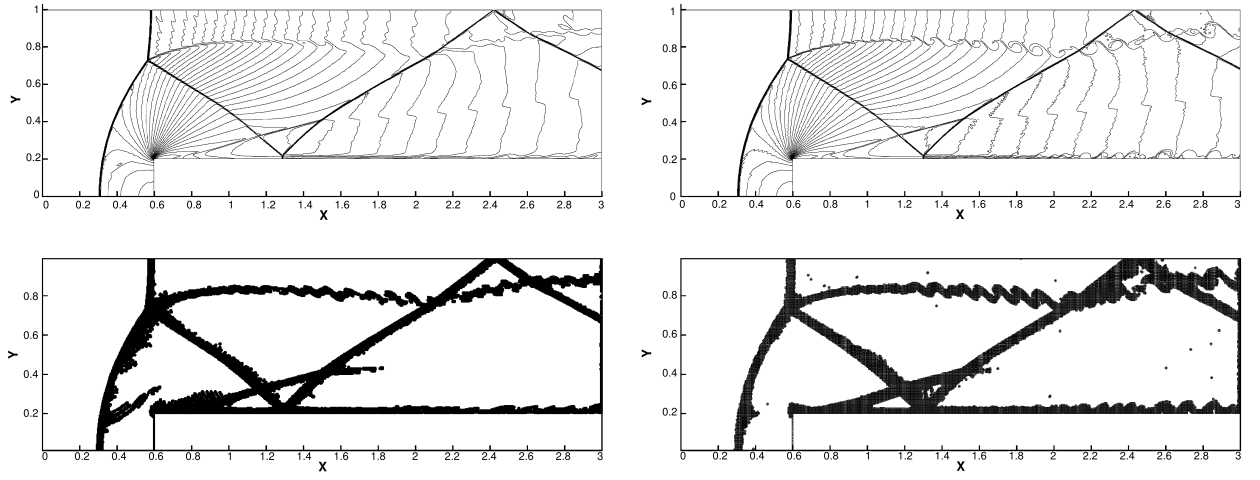

Fig. 3.11. Forward step problem. $T = 4$. From top to bottom: 30 equally spaced density contours from 0.32 to 6.15; the locations of the troubled-cells at the final time. The hybrid HWENO scheme (left); the new hybrid HWENO scheme (right). Uniform meshes with 960×320 cells.

is up to $T = 4$, then, we present the computed density and the locations of the troubled-cells at the final time in Fig. 3.11. We notice that the new hybrid HWENO scheme has high resolutions than the hybrid HWENO scheme, and it also has bigger CFL number, less candidate stencils, higher order numerical accuracy and simpler HWENO methodology. Similarly, only a small part of cells are identified as troubled-cells, and it means that most regions directly use linear approximation, which can increase the efficiency obviously.

4. Concluding remarks

In this paper, a new fifth-order hybrid finite volume Hermite weighted essentially non-oscillatory (HWENO) scheme with artificial linear weights is designed for solving hyperbolic conservation laws. Compared with the hybrid HWENO scheme [44], we employ a nonlinear convex combination of a high degree polynomial with several low degree polynomials in the new HWENO reconstruction, and the associated linear weights can be any artificial positive numbers (their sum is one), which would have the advantages of its simplicity and easy extension to multi-dimension. Meanwhile, different choice of the linear weights would not affect the numerical accuracy, and it gets smaller numerical errors than the original HWENO methodology. In addition, the new hybrid HWENO scheme has higher order numerical accuracy in two dimension. Moreover, the scheme still keeps the non-oscillations as we apply the limiter methodology for the first order moments in the troubled-cells and use new HWENO reconstruction on the interface. In the implementation, only a small part of cells are identified as troubled-cells, which means that most regions directly use linear approximation. For the spatial discretization, the HWENO schemes are more compact than the classical fifth order WENO schemes [22,36] as only immediate neighbor information is needed in the reconstruction, and the new hybrid HWENO scheme also has higher efficiency than WENO scheme with smaller numerical errors. In short, the new hybrid HWENO scheme has high resolution, efficiency, non-oscillation and robustness, simultaneously, and these numerical results also show its good performances. The extension of the method to unstructured meshes is going on.

Declaration of competing interest

The authors declare that they have no known competing financial interests or personal relationships that could have appeared to influence the work reported in this paper.

References

[1] D.S. Balsara, Self-adjusting, positivity preserving high order schemes for hydrodynamics and magnetohydrodynamics, J. Comput. Phys. 231 (2012) 7504–7517.
[2] W. Boscheri, D.S. Balsara, High order direct arbitrary-Lagrangian-Eulerian (ALE) $P_N P_M$ schemes with WENO adaptive-order reconstruction on unstructured meshes, J. Comput. Phys. 398 (2019) 108899.
[3] W. Boscheri, M. Dumbser, R. Loubère, P.H. Maire, A second-order cell-centered Lagrangian ADER-MOOD finite volume scheme on multidimensional unstructured meshes for hydrodynamics, J. Comput. Phys. 358 (2018) 103–129.
[4] D.S. Balsara, S. Garain, V. Florinski, W. Boscheri, An efficient class of WENO schemes with adaptive order for unstructured meshes, J. Comput. Phys. 404 (2020) 109062.
[5] D.S. Balsara, S. Garain, C.-W. Shu, An efficient class of WENO schemes with adaptive order, J. Comput. Phys. 326 (2016) 780–804.
[6] M. Castro, B. Costa, W.S. Don, High order weighted essentially non-oscillatory WENO-Z schemes for hyperbolic conservation laws, J. Comput. Phys. 230 (2011) 1766–1792.
[7] B. Costa, W.S. Don, Multi-domain hybrid spectral-WENO methods for hyperbolic conservation laws, J. Comput. Phys. 224 (2007) 970–991.
[8] B. Costa, W.S. Don, High order Hybrid Central-WENO finite difference scheme for conservation laws, J. Comput. Appl. Math. 204 (2007) 209–218.
[9] S. Clain, S. Diot, R. Loubère, A high-order finite volume method for systems of conservation laws - multi-dimensional optimal order detection (MOOD), J. Comput. Phys. 230 (2011) 4028–4050.
[10] B. Cockburn, C.-W. Shu, TVB Runge-Kutta local projection discontinuous Galerkin finite element method for conservation laws II: general framework, Math. Comput. 52 (1989) 411–435.
[11] X. Cai, X. Zhang, J. Qiu, Positivity-preserving high order finite volume HWENO schemes for compressible Euler equations, J. Sci. Comput. 68 (2016) 464–483.
[12] M. Dumbser, W. Boscheri, M. Semplice, G. Russo, Central weighted ENO schemes for hyperbolic conservation laws on fixed and moving unstructured meshes, SIAM J. Sci. Comput. 39 (2017) A2564–A2591.
[13] M. Dumbser, D.S. Balsara, E.F. Toro, C.D. Munz, A unified framework for the construction of one-step finite volume and discontinuous Galerkin schemes on unstructured meshes, J. Comput. Phys. 227 (2008) 8209–8253.
[14] S. Diot, S. Clain, R. Loubère, Improved detection criteria for the multi-dimensional optimal order detection (MOOD) on unstructured meshes with very high-order polynomials, Comput. Fluids 64 (2012) 43–63.
[15] S. Diot, R. Loubère, S. Clain, The MOOD method in the three-dimensional case: very-high-order finite volume method for hyperbolic systems, Int. J. Numer. Methods Fluids 73 (2013) 362–392.
[16] G.S. Fu, C.-W. Shu, A new troubled-cell indicator for discontinuous Galerkin methods for hyperbolic conservation laws, J. Comput. Phys. 347 (2017) 305–327.
[17] A. Harten, Preliminary results on the extension of ENO schemes to two-dimensional problems, in: C. Carasso, et al. (Eds.), Proceedings, International Conference on Nonlinear Hyperbolic Problems, Saint-Etienne, 1986, in: Lecture Notes in Mathematics, Springer-Verlag, Berlin, 1987.
[18] A. Harten, B. Engquist, S. Osher, S. Chakravarthy, Uniformly high order accurate essentially non-oscillatory schemes III, J. Comput. Phys. 71 (1987) 231–323.
[19] A. Harten, S. Osher, Uniformly high-order accurate non-oscillatory schemes, IMRC Technical Summary Rept. 2823, Univ. of Wisconsin, Madison, WI, May 1985.
[20] D.J. Hill, D.I. Pullin, Hybrid tuned center-difference-WENO method for large eddy simulations in the presence of strong shocks, J. Comput. Phys. 194 (2004) 435–450.
[21] C. Hu, C.-W. Shu, Weighted essentially non-oscillatory schemes on triangular meshes, J. Comput. Phys. 150 (1999) 97–127.
[22] G.-S. Jiang, C.-W. Shu, Efficient implementation of weighted ENO schemes, J. Comput. Phys. 126 (1996) 202–228.
[23] L. Krivodonova, J. Xin, J.-F. Remacle, N. Chevaugeon, J.E. Flaherty, Shock detection and limiting with discontinuous Galerkin methods for hyperbolic conservation laws, Appl. Numer. Math. 48 (2004) 323–338.
[24] H. Luo, J.D. Baum, R. Lohner, A Hermite WENO-based limiter for discontinuous Galerkin method on unstructured grids, J. Comput. Phys. 225 (2007) 686–713.
[25] X.D. Liu, S. Osher, T. Chan, Weighted essentially non-oscillatory schemes, J. Comput. Phys. 115 (1994) 200–212.

[26] D. Levy, G. Puppo, G. Russo, Central WENO schemes for hyperbolic systems of conservation laws, Math. Model. Numer. Anal. 33 (1999) 547–571.
[27] D. Levy, G. Puppo, G. Russo, Compact central WENO schemes for multidimensional conservation laws, SIAM J. Sci. Comput. 22 (2000) 656–672.
[28] G. Li, J. Qiu, Hybrid weighted essentially non-oscillatory schemes with different indicators, J. Comput. Phys. 229 (2010) 8105–8129.
[29] H. Liu, J. Qiu, Finite difference Hermite WENO schemes for conservation laws, J. Sci. Comput. 63 (2015) 548–572.
[30] S. Pirozzoli, Conservative hybrid compact-WENO schemes for shock-turbulence interaction, J. Comput. Phys. 178 (2002) 81–117.
[31] J. Qiu, C.-W. Shu, Hermite WENO schemes and their application as limiters for Runge-Kutta discontinuous Galerkin method: one-dimensional case, J. Comput. Phys. 193 (2004) 115–135.
[32] J. Qiu, C.-W. Shu, Hermite WENO schemes and their application as limiters for Runge-Kutta discontinuous Galerkin method II: two dimensional case, Comput. Fluids 34 (2005) 642–663.
[33] J. Qiu, C.-W. Shu, Runge-Kutta discontinuous Galerkin method using WENO limiters, SIAM J. Sci. Comput. 26 (2005) 907–929.
[34] J. Qiu, C.-W. Shu, A comparison of trouble cell indicators for Runge-Kutta discontinuous Galerkin method using WENO limiters, SIAM J. Sci. Comput. 27 (2005) 995–1013.
[35] D. Ray, J.S. Hesthaven, An artificial neural network as a troubled-cell indicator, J. Comput. Phys. 367 (2018) 166–191.
[36] C.-W. Shu, Essentially non-oscillatory and weighted essentially non-oscillatory schemes for hyperbolic conservation laws, in: A. Quarteroni (Ed.), Advanced Numerical Approximation of Nonlinear Hyperbolic Equations, in: Lecture Notes in Mathematics, CIME Subseries, Springer, Berlin, 1998.
[37] J. Shi, C. Hu, C.-W. Shu, A technique of treating negative weights in WENO schemes, J. Comput. Phys. 175 (2002) 108–127.
[38] C.-W. Shu, S. Osher, Efficient implementation of essentially non-oscillatory shock capturing schemes, J. Comput. Phys. 77 (1988) 439–471.
[39] Z. Tao, F. Li, J. Qiu, High-order central Hermite WENO schemes on staggered meshes for hyperbolic conservation laws, J. Comput. Phys. 281 (2015) 148–176.
[40] Z. Tao, F. Li, J. Qiu, High-order central Hermite WENO schemes: dimension-by-dimension moment-based reconstructions, J. Comput. Phys. 318 (2016) 222–251.
[41] M.J. Vuik, J.K. Ryan, Multiwavelet troubled-cell indicator for discontinuity detection of discontinuous Galerkin schemes, J. Comput. Phys. 270 (2014) 138–160.
[42] P. Woodward, P. Colella, The numerical simulation of two-dimensional fluid flow with strong shocks, J. Comput. Phys. 54 (1984) 115–173.
[43] Y.H. Zahran, A.H. Abdalla, Seventh order Hermite WENO scheme for hyperbolic conservation laws, Comput. Fluids 131 (2016) 66–80.
[44] Z. Zhao, Y. Chen, J. Qiu, A hybrid Hermite WENO scheme for hyperbolic conservation laws, J. Comput. Phys. 405 (2020) 109175.
[45] J. Zhu, J. Qiu, A class of forth order finite volume Hermite weighted essentially non-oscillatory schemes, Sci. China Ser. A, Math. 51 (2008) 1549–1560.
[46] J. Zhu, J. Qiu, A new fifth order finite difference WENO scheme for solving hyperbolic conservation laws, J. Comput. Phys. 318 (2016) 110–121.
[47] J. Zhu, J. Qiu, A new type of finite volume WENO schemes for hyperbolic conservation laws, J. Sci. Comput. 73 (2017) 1338–1359.
[48] J. Zhu, J. Qiu, A new third order finite volume weighted essentially non-oscillatory scheme on tetrahedral meshes, J. Comput. Phys. 349 (2017) 220–232.
[49] J. Zhu, J. Qiu, A simple finite volume weighted essentially non-oscillatory schemes on triangular meshes, SIAM J. Sci. Comput. 40 (2018) A903–A928.
[50] J. Zhu, J. Qiu, C.-W. Shu, High-order Runge-Kutta discontinuous Galerkin methods with a new type of multi-resolution WENO limiters, J. Comput. Phys. 404 (2020) 109105.
[51] Z. Zhao, J. Zhu, Y. Chen, J. Qiu, A new hybrid WENO scheme for hyperbolic conservation laws, Comput. Fluids 179 (2019) 422–436.
[52] J. Zhu, X. Zhong, C.-W. Shu, J. Qiu, Runge-Kutta discontinuous Galerkin method with a simple and compact Hermite WENO limiter, Commun. Comput. Phys. 19 (2016) 944–969.